Trapping and recombination via dangling bonds in amorphous and glassy semiconductors under steady-state conditions: Application to the modulated photocurrent experiment

C. Longeaud and J. P. Kleider
Laboratoire de Génie Electrique de Paris, Ecole Supérieure d'Electricité, Universités Paris VI et Paris XI, Plateau de Moulon, 91192 Gif-sur-Yvette Cedex, France
(Received 3 May 1993)

Interesting features of the modulated photocurrent experiment have been emphasized in a recent paper where we have shown that, if the localized states in the gap belong to the same species of monovalent centers, then it is possible to deduce both an order of magnitude of the capture cross section and the absolute value of the density of these states by means of this experiment. In the present paper, we extend the calculation of the dc and ac photocurrent to the case where distributions of correlated states associated with the well-known dangling bonds (DB) are present in the material. This calculation includes the contributions of both holes and electrons and takes into account the interactions of both types of carriers with distributions of monovalent as well as correlated states in the gap of a semiconductor. We concentrate in particular on the signature of the DB states in the data analysis, the correlation energy being either positive or negative. We first derive the variations with respect to energy of the occupation functions of any distribution of DB states for both signs of the correlation energy under steady-state conditions. We show that the concept of quasi-Fermi-levels for trapped carriers introduced by Simmons and Taylor for monovalent states has to be reconsidered for the correlated states and we underline the differences between the cases of positive and negative correlation energies. We give a clear and comprehensive scheme of the different recombination paths for the correlated states and derive the correct expressions of the electron and hole lifetimes related to these kinds of states. The results of the steady-state-regime study are then used in a second part to identify how the DB states modify the modulated photocurrent. Simplified expressions of the modulus of the modulated photocurrent and of its phase shift with reference to the ac excitation light are given in two cases: a recombination-limited regime and a trapping- and release-limited regime. The behaviors of the modulated photocurrent related to the presence of DB states are also underlined in both regimes by means of a numerical simulation. It is shown that a distribution of DB centers exhibiting a positive correlation energy roughly behaves as *two* distributions of monovalent states whereas a distribution of DB centers with a negative correlation energy roughly behaves as a *single* distribution of monovalent states. An important property of the DB states with a positive correlation energy is that they can give a significant response in the trapping- and release-limited regime even if their ground-energy level is below the Fermi level. It is also shown that if there are both monovalent- and correlated-state distributions in the gap, it is possible to derive an order of magnitude of the lowest capture cross sections from the transition between the recombination-limited and trapping- and release-limited regimes.

I. INTRODUCTION

The determination of the density of localized states present in the mobility gap of amorphous or glassy semiconductors is still a matter of research, but the theoretical and experimental work performed so far has led to a general picture which is commonly accepted by most of the authors. In this picture part of the density of states (DOS) is made of conduction- and valence-band tails of localized states,[1,2] usually assumed as monovalent (i.e., being neutral or singly charged), that originate from the disorder intrinsic to such materials. Deeper in the gap are other states, usually attributed to dangling bonds (DB), that can be positively charged (D^+), neutral (D^0), or negatively charged (D^-) if occupied by zero, one, or two electrons, respectively.[3] This kind of defect is described in the energy domain by two levels E_{DB} and $E_{DB}+E_u$ where E_u is the correlation energy. The sign and the value of the correlation energy depend on the material considered. It is generally accepted that the correlation energy is negative in chalcogenide glasses such as a-As_2Se_3,[4] whereas it is positive in tetrahedrally bounded amorphous semiconductors such as a-Si:H.[5,6] Though their origin is still a matter of controversy,[7–10] the DB states play an essential role in the material properties and they are included in almost all the models invoked as an explanation for the results of any experiment performed on amorphous or glassy semiconductors. For instance, their influence on the steady-state photoconductivity has been widely studied[11,12] and is still studied.[13] These states are also involved in the thermal equilibrium processes observed in a-Si:H,[14–16] as well as in the light-induced metastabilities known as the Staebler-Wronsky effect (for a recent review see, for instance, Zellama *et al.*[17]).

However, the inclusion of DB states in the analysis of

0163-1829/93/48(12)/8715(27)/$06.00

experimental results is often restrictive. They are mainly considered as discrete levels[18] instead of distributions of states, and, apparently because of the complexity of the calculation linked to their specific statistics,[19,20] they are often treated as monovalent states[21] by means of well-known statistics such as the one extensively studied by Simmons and Taylor.[22] We present in this paper a detailed and comprehensive analysis of the energy dependence of the DB states occupancy under steady-state illumination conditions. We show that simplified expressions of the occupation functions can be found depending on the considered energy range, and we give a comprehensive view of the recombination paths along with the corresponding expressions for the recombination rates of electrons and holes.

Among all the experiments performed on amorphous and glassy semiconductors to study the DOS, the modulated photocurrent (MPC) experiment is both powerful and convenient. Indeed, this experiment has been applied to CdS crystals by its inventor,[23] and then to *a*-Si:H (Refs. 24 and 25) and to *a*-As_2Se_3.[26,27] However, to our knowledge, among all the attempts to correlate the experimental results with the presence of DB states in the mobility gap, only a few have been made by means of the basic equations.[23,27] In a previous paper, we have presented a detailed calculation and analysis of the modulated photocurrent including the contributions of holes and electrons for the case where the DOS consists of a single species of monovalent states.[28] In the present paper we extend this calculation to densities of states, which also includes distributions of DB states, and we emphasize the part of the calculation relative to these states. The cases of positive as well as negative correlation energies are addressed. Obviously, since the MPC experiment is mainly performed on samples built in the coplanar geometry, both types of carriers, electrons and holes, are taken into account.

In Sec. II, we present the whole calculation starting from the basic continuity equations which are recalled in Sec. II A. In order to simplify the treatment of the problem, we consider distributions of DB centers having a constant correlation energy E_u. If there is a repartition of correlation energies associated with the defect distribution, as suggested by some authors,[29] one can always divide the whole DB state into DB distributions with constant E_u. In Sec. II B, a treatment of the dc contribution to the current is given which emphasizes the part due to the DB states. This treatment, presenting some similarities to that of monovalent states described by Simmons and Taylor,[22,30] is achieved for $E_u>0$ and for $E_u<0$. In Sec. II C, the whole treatment of the alternative part of the photocurrent is presented for the two cases ($E_u>0$ and $E_u<0$). The experimental differences expected in both cases are underlined.

In Sec. III, the approximate analytical results of Sec. II C are tested and illustrated by means of a numerical simulation. Particular attention is paid to the transition from a recombination-limited regime of the modulated photocurrent to a trapping- and release-limited regime and to the possibility of reconstructing the DOS in the presence of DB states. We emphasize the insights that the MPC experiment can bring to the defects in amorphous and glassy semiconductors.

II. THEORY

A. Basic equations

We consider a semiconductor layer in a coplanar configuration uniformly illuminated so that the densities of electrons and holes in the extended states (n and p, respectively) are uniform in the conduction cross-sectional area S. The general expression for the current I is then given by

$$I=Sq\xi(\mu_n n+\mu_p p)\ , \tag{1}$$

where q is the absolute value of the electronic charge, ξ is the applied electric field, and μ_n and μ_p are the extended states mobilities of electrons and holes, respectively.

The values of n and p can be obtained from the resolution of continuity equations, taking the different emission and capture processes into account. In the following we shall consider a DOS made of two types of states: a single species of monovalent traps and a single species of DB states.

A species of *monovalent* traps is defined by capture cross sections for electrons and holes, σ_n and σ_p, respectively, and a density of states $N(E)$ at the energy E. The statistics of occupation of such states was presented by Simmons and Taylor[22] as an extension of the Shockley-Read[31] statistics, where it is assumed that localized states can only exchange carriers via the extended states.

A species of *dangling bonds* states is defined by a density of states $N^{\mathrm{DB}}(E)$, the capture cross sections for electrons σ_n^0 and σ_n^+ of the D^0 and D^+ states, respectively, the capture cross sections for holes σ_p^0 and σ_p^- of the D^0 and D^- states, respectively, and a correlation energy E_u. The occupancy of these centers follows the statistics of correlated states[19,20] instead of Fermi-Dirac statistics. We also assume that this type of state can only exchange carriers via the extended states.

We have to keep in mind that a real DOS can be composed of more than one species of each type of states. However, from a mathematical point of view the formalism used in the equations does not depend on the number of species involved and the choice of a single species of both monovalent and dangling-bond states is made to clarify the development.

The electron and hole current densities being uniform, and calling t the time, G the generation rate of carriers (G being the same for electrons and holes since we consider only photon energies greater than the mobility gap), E_c the energy of the bottom of the conduction band, and E_v the energy of the top of the valence band, the continuity equations for electrons and holes are

$$\frac{\partial n}{\partial t}=G-\int_{E_v}^{E_c}N(E)\{\bar{n}[1-f(E)]-e_n(E)f(E)\}dE$$
$$+\int_{E_v}^{E_c}N^{\mathrm{DB}}(E)[e_n^-(E)f^-(E)-(\bar{n}^{\,0}-e_n^0)f^0(E)$$
$$-\bar{n}^{\,+}f^+(E)]dE \tag{2}$$

and

$$\frac{\partial p}{\partial t}=G-\int_{E_v}^{E_c}N(E)\{\bar{p}f(E)-e_p(E)[1-f(E)]\}dE + \int_{E_v}^{E_c}N^{\mathrm{DB}}(E)[e_p^{+}(E)f^{+}(E)-(\bar{p}^{\,0}-e_p^{0})f^{0}(E) -\bar{p}^{\,-}f^{-}(E)]dE \ . \tag{3}$$

The first and second integrals in Eqs. (2) and (3) describe the interactions of electrons and holes with the monovalent states and the DB states, respectively. In these equations the notations relevant to the monovalent traps are the following: $f(E)$, the probability of the states at the energy E to be occupied by an electron; $e_n(E)$ and $e_p(E)$, the emission rates of electrons and holes from a state at the energy E toward the conduction and valence band, respectively; and $\bar{n}$ and $\bar{p}$, the capture rates of electrons and holes which can be written $\bar{n}=v_n\sigma_n n=c_n n$ and $\bar{p}=v_p\sigma_p p=c_p p$, v_n and v_p being the thermal velocities and c_n and c_p the corresponding capture coefficients for electrons and holes, respectively.

The notations relevant to the DB states are the following: $f^{+}(E)$, $f^{0}(E)$, and $f^{-}(E)$, the probabilities of a DB center at the energy E to be positively charged, neutral, and negatively charged, respectively; e_n^{0} and e_n^{-}, the emission rates of electrons toward the conduction band from neutral and negatively charged states; e_p^{0} and e_p^{+}, the emission rates of holes toward the valence band from neutral and positively charged states; $\bar{n}^{\,0}$ and $\bar{n}^{\,+}$, the capture rates of electrons by neutral and positively charged states; $\bar{p}^{\,0}$ and $\bar{p}^{\,-}$, the capture rates of holes by neutral and negatively charged states. These capture rates can be written $\bar{n}^{\,0}=v_n\sigma_n^{0}n$, $\bar{n}^{\,+}=v_n\sigma_n^{+}n$, $\bar{p}^{\,0}=v_p\sigma_p^{0}p$, and $\bar{p}^{\,-}=v_p\sigma_p^{-}p$. The corresponding capture coefficients for electrons and holes can be defined exactly as for the monovalent states (e.g., $c_n^{+}=v_n\sigma_n^{+}$).

According to the Shockley-Read[31] formalism the occupation functions are given by

$$\frac{\partial f(E)}{\partial t}=\bar{n}+e_p(E)-f(E)[\bar{n}+\bar{p}+e_n(E)+e_p(E)] \ ,$$
$$\frac{\partial f^{-}(E)}{\partial t}=[\bar{n}^{\,0}+e_p^{0}(E)]f^{0}(E)-[\bar{p}^{\,-}+e_n^{-}(E)]f^{-}(E) \ , \tag{4}$$
$$\frac{\partial f^{+}(E)}{\partial t}=[\bar{p}^{\,0}+e_n^{0}(E)]f^{0}(E)-[\bar{n}^{\,+}+e_p^{+}(E)]f^{+}(E) \ ,$$
$$1=f^{+}(E)+f^{0}(E)+f^{-}(E) \ .$$

Since in the MPC experiment the excitation light is a periodic function of the time, two types of contributions have to be considered: the first one giving a dc current due to the average contribution of the excitation to the creation of carriers and the second one coming from the alternative part of the excitation. We treat the case of a small ac signal and do not take the harmonics into consideration. So, basically all the quantities appearing in Eqs. (2)–(4), except the emission rates and the distributions of states, can be separated in two components indexed dc for the steady-state component and ac for the alternative component $Q=Q_{\mathrm{dc}}+Q_{\mathrm{ac}}\exp(j\omega t)$, where j is the complex quantity such that $j^2=-1$ and ω is the pulsation of the excitation. Taking both the dc and ac components into account, Eqs. (2)–(4) can be split into equations including the dc and ac contributions, respectively. For the steady-state contribution, we obtain

$$0=G_{\mathrm{dc}}-\int_{E_v}^{E_c}N(E)\{\bar{n}_{\mathrm{dc}}[1-f_{\mathrm{dc}}(E)]-e_n(E)f_{\mathrm{dc}}(E)\}dE + \int_{E_v}^{E_c}N^{DB}(E)\{e_n^{-}(E)f_{\mathrm{dc}}^{-}(E)-\bar{n}_{\mathrm{dc}}^{+}f_{\mathrm{dc}}^{+}(E) -[\bar{n}_{\mathrm{dc}}^{0}-e_n^{0}(E)]f_{\mathrm{dc}}^{0}(E)\}dE \tag{5}$$

and

$$0=G_{\mathrm{dc}}-\int_{E_v}^{E_c}N(E)\{\bar{p}_{\mathrm{dc}}f_{\mathrm{dc}}(E)-e_p(E)[1-f_{\mathrm{dc}}(E)]\}dE + \int_{E_v}^{E_c}N^{\mathrm{DB}}(E)\{e_p^{+}(E)f_{\mathrm{dc}}^{+}(E)-\bar{p}_{\mathrm{dc}}^{-}f_{\mathrm{dc}}^{-}(E) -[\bar{p}_{\mathrm{dc}}^{0}-e_p^{0}(E)]f_{\mathrm{dc}}^{0}(E)\}dE \ . \tag{6}$$

For the alternative contribution, we obtain

$$j\omega n_{\mathrm{ac}}=G_{\mathrm{ac}}+\int_{E_v}^{E_c}N(E)\{[n_{\mathrm{dc}}+e_n(E)]f_{\mathrm{ac}}(E)-\bar{n}_{\mathrm{ac}}[1-f_{\mathrm{dc}}(E)]\}dE + \int_{E_v}^{E_c}N^{\mathrm{DB}}(E)[e_n^{-}(E)f_{\mathrm{ac}}^{-}(E)-\bar{n}_{\mathrm{dc}}^{+}f_{\mathrm{ac}}^{+}(E)-\bar{n}_{\mathrm{ac}}^{+}f_{\mathrm{dc}}^{+}(E)]dE - \int_{E_v}^{E_c}N^{\mathrm{DB}}(E)\{\bar{n}_{\mathrm{ac}}^{0}f_{\mathrm{dc}}^{0}(E)+[\bar{n}_{\mathrm{dc}}^{0}-e_n^{0}(E)]f_{\mathrm{ac}}^{0}(E)\}dE \tag{7}$$

and

$$j\omega p_{\mathrm{ac}}=G_{\mathrm{ac}}-\int_{E_v}^{E_c}N(E)\{[p_{\mathrm{dc}}+e_p(E)]f_{\mathrm{ac}}(E)+\bar{p}_{\mathrm{ac}}f_{\mathrm{dc}}(E)\}dE+\int_{E_v}^{E_c}N^{\mathrm{DB}}(E)[e_p^{+}(E)f_{\mathrm{ac}}^{+}(E)-\bar{p}_{\mathrm{dc}}^{-}f_{\mathrm{ac}}^{-}(E)-\bar{p}_{\mathrm{ac}}^{-}f_{\mathrm{dc}}^{-}(E)]dE$$
$$-\int_{E_v}^{E_c}N^{\mathrm{DB}}(E)\{\bar{p}_{\mathrm{ac}}^{0}f_{\mathrm{dc}}^{0}(E)+[\bar{p}_{\mathrm{dc}}^{0}-e_p^{0}(E)]f_{\mathrm{ac}}^{0}(E)\}dE \ . \tag{8}$$

From these equations it is possible to deduce n_{dc}, p_{dc}, n_{ac}, and p_{ac}, taking account of the charge neutrality given by

$$\begin{aligned}(p_{dc}-p_{dc0})-(n_{dc}-n_{dc0})&=\int_{E_v}^{E_c}N^{DB}(E)\{[f^0_{dc}(E)-f^0_{dc0}(E)]\\&\quad+2[f^-_{dc}(E)-f^-_{dc0}(E)]\}dE\\&\quad+\int_{E_v}^{E_c}N(E)[f_{dc}(E)-f_{dc0}(E)]dE\ ,\end{aligned}\tag{9}$$

where the subscript 0 indicates that the quantities considered correspond to the dark thermal equilibrium.

Note that if we assume that $N^{DB}(E)=0$, then Eqs. (5)–(9) transform into Eqs. (5)–(8) and (12) of a previous paper.[28] In that paper the case of the monovalent states was treated extensively. Therefore, in the following, we shall concentrate on the part of the equations involving the DB states: this is done by equating $N(E)$ to zero.

As Okamoto, Kida, and Hamakawa did,[12] if we write, for the sake of simplicity,

$$\begin{aligned}N^+(E)&=\bar{n}^+_{dc}+e_p^+(E)\ ,\\N^0(E)&=\bar{n}^0_{dc}+e_p^0(E)\ ,\\P^0(E)&=\bar{p}^0_{dc}+e_n^0(E)\ ,\\P^-(E)&=\bar{p}^-_{dc}+e_n^-(E)\ ,\end{aligned}\tag{10}$$

the last three equations of the system of equations (4) transform into two subsystems: one for the dc components,

$$\begin{aligned}&N^0(E)f^0_{dc}(E)-P^-(E)f^-_{dc}(E)=0\ ,\\&P^0(E)f^0_{dc}(E)-N^+(E)f^+_{dc}(E)=0\ ,\\&f^-_{dc}(E)+f^0_{dc}(E)+f^+_{dc}(E)=1\ ,\end{aligned}\tag{11}$$

and another one for the ac components,

$$\begin{aligned}&N^0(E)f^0_{ac}(E)+\bar{n}^0_{ac}f^0_{dc}(E)-\bar{p}^-_{ac}f^-_{dc}(E)=f^-_{ac}(E)[j\omega+P^-(E)]\ ,\\&P^0(E)f^0_{ac}(E)+\bar{p}^0_{ac}f^0_{dc}(E)-\bar{n}^+_{ac}f^+_{dc}(E)=f^+_{ac}(E)[j\omega+N^+(E)]\ ,\\&f^+_{ac}(E)+f^0_{ac}(E)+f^-_{ac}(E)=0\ .\end{aligned}\tag{12}$$

From the first subsystem one obtains the expressions of f^+_{dc}, f^0_{dc}, and f^-_{dc},

$$\begin{aligned}f^+_{dc}&=\frac{P^0P^-}{P^0P^-+N^+P^-+N^0N^+}\ ,\\f^0_{dc}&=\frac{N^+}{P^0}f^+_{dc},\quad f^-_{dc}=\frac{N^0}{P^-}f^0_{dc}\ ,\end{aligned}\tag{13}$$

as functions of the different emission and capture rates for a given energy. These equations have been obtained already and extensively used by some authors for the study of the photoconduction (see, for instance, Vaillant and Jousse,[11] Vaillant, Jousse, and Bruyère,[32] and Okamoto, Kida, and Hamakawa[12]). Nevertheless, the study of the alternative part, which is essential for the calculation of the modulated photocurrent, requires the complete knowledge of the variations of the dc occupation functions with respect to the energy. This point is addressed in the next subsection where we derive the detailed energy dependence of the occupation functions and give simple approximate expressions of these functions in both cases $E_u>0$ and $E_u<0$. This will be done essentially by making a parallel between our calculation for the DB centers and that for monovalent states, using the formalism of Simmons and Taylor.[22]

Before going further, it is worth noticing that the expression of f^-_{dc} in Eqs. (13) is obtained from the expression of f^+_{dc} by a simple transformation of notations called $\mathcal{T}$ in the following: changing all the letters N or n into P or p (all the P or p into N or n) and all the superscripts $-$ into $+$ (all the superscripts $+$ into $-$) transforms the expression of f^+_{dc} into that of f^-_{dc}, the expression of f^0_{dc} being unchanged by $\mathcal{T}$. The interest of this transformation in order to simplify and shorten the calculation will appear immediately.

From the second subsystem we deduce the expressions of f^+_{ac}, f^0_{ac}, and f^0_{ac} as functions of n_{ac} and p_{ac}. Since there is a phase shift between the alternative component of the light of excitation and the modulated photocurrent these last quantities are complex, and we can write $n_{ac}=n_r+jn_i$, $p_{ac}=p_r+jp_i$, the indices r and i standing for real and imaginary, respectively. Then, the expressions of f^+_{ac}, f^0_{ac}, and f^-_{ac} at an energy E are

$$\begin{aligned}f^+_{ac}(E)&=n_r\alpha_n^++n_i\beta_n^++p_r\alpha_p^++p_i\beta_p^+\\&\quad+j(-n_r\beta_n^++n_i\alpha_n^+-p_r\beta_p^++p_i\alpha_p^+)\ ,\\f^0_{ac}(E)&=n_r\alpha_n^0+n_i\beta_n^0+p_r\alpha_p^0+p_i\beta_p^0\\&\quad+j(-n_r\beta_n^0+n_i\alpha_n^0-p_r\beta_p^0+p_i\alpha_p^0)\ ,\\f^-_{ac}(E)&=n_r\alpha_n^-+n_i\beta_n^-+p_r\alpha_p^-+p_i\beta_p^-\\&\quad+j(-n_r\beta_n^-+n_i\alpha_n^--p_r\beta_p^-+p_i\alpha_p^-)\ ,\end{aligned}\tag{14}$$

where the expressions of the energy-dependent coefficients of n_r, n_i, p_r, and p_i for each function are given in Appendix A. As an example of the usefulness of $\mathcal{T}$, note that the application of $\mathcal{T}$ to the expression of f^+_{ac} in Eqs. (14) gives the expression of f^-_{ac}.

B. Study of the dc contribution

The formalism of Simmons and Taylor[22] has been proved to successfully explain and describe the variations with respect to the energy of the occupation functions of monovalent traps within the gap of a semiconductor under nonequilibrium steady-state conditions. In this section we show that an equivalent formalism can be applied to a distribution of correlated states such as DB states and, consequently, that one can obtain the variations with respect to the energy of the steady-state occupation functions f^+_{dc}, f^0_{dc}, and f^-_{dc} within the gap of a semiconductor. Because the ac components of the main physical quantities depend on their dc components, the study of these variations is essential for the determination of f^+_{ac},

f^0_{ac}, and f^-_{ac}, which in turn determine the ac components of the densities of free carriers, and hence the modulated photocurrent.

The variations of the occupation functions with respect to the energy under dark thermal equilibrium conditions were presented by Okamoto and Hamakawa[20] several years ago for both cases $E_u > 0$ and $E_u < 0$. These variations are recalled in Figs. 1(a) and 1(b), respectively. As seen in these figures, both cases are not symmetrical. In the case $E_u < 0$, two intervals can be roughly defined, one for which $f^+_{dc0} = 1$ and one for which $f^-_{dc0} = 1$, f^0_{dc0} being practically always negligible. In the case $E_u > 0$ three intervals, wherein each function is alternatively roughly equal to 1, can be defined. In both cases the limits of these intervals depend on the position of the dark Fermi level and of the correlation energy.

Under illumination we expect the dark Fermi level E_F to split into a quasi-Fermi-level for electrons E_{Fn} and a quasi-Fermi-level for holes E_{Fp}. Therefore, in the case $E_u < 0$ we expect to observe at the most three different intervals wherein the occupation functions take different values, whereas in the case $E_u > 0$, we expect to observe at the most five different intervals wherein the occupation functions take different values.

Calling N_c and N_v the equivalent densities of states at the bottom of the conduction and top of the valence band, respectively, n_{dc} and p_{dc} are written

$$n_{dc} = N_c \exp\left[-\frac{E_c - E_{Fn}}{k_B T}\right],$$
$$p_{dc} = N_v \exp\left[-\frac{E_{Fp} - E_v}{k_B T}\right], \tag{15}$$

where k_B is the Boltzmann constant and T the temperature. Under conditions such that $n_{dc} \gg n_{dc0}$ and $p_{dc} \gg p_{dc0}$, the electron lifetime τ_n and the hole lifetime

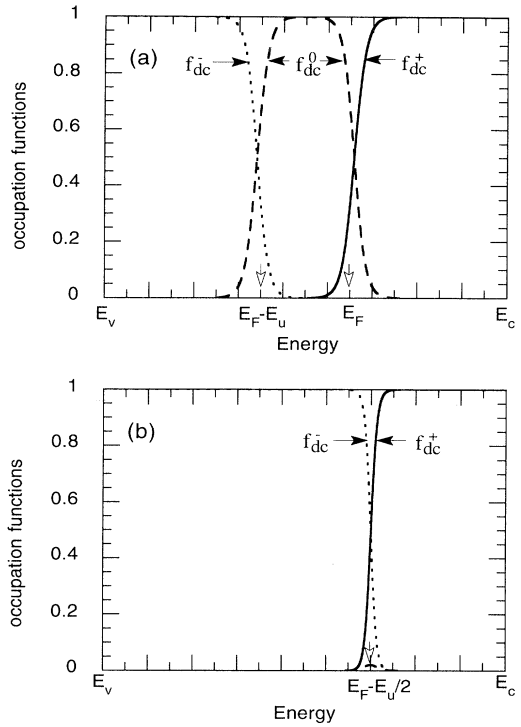

FIG. 1. Variations of the occupation functions f^+_{dc}, f^0_{dc}, and f^-_{dc} (full, dashed, and dotted lines, respectively) vs the energy under dark thermal equilibrium in the cases (a) $E_u > 0$ and (b) $E_u < 0$. Characteristic energies of these variations are indicated by open arrows along the energy axis in both figures. Whereas three different regions are distinguishable in the case $E_u > 0$, only two regions exist in the case $E_u < 0$. In this last case, $f^0_{dc}(E)$ never takes significant values provided that $|E_u| \gg k_B T$.

τ_p are usually defined by $G_{dc} = n_{dc}/\tau_n$ and $G_{dc} = p_{dc}/\tau_p$, respectively. After some calculations, the parts relative to the dangling-bond states τ_n^{DB} and τ_p^{DB} can be written independently of the sign of the correlation energy,

$$\frac{1}{\tau_n^{DB}} = \int_{E_v}^{E_c} \left[\frac{c_n^+ \bar{p}^0_{dc}[\bar{p}^-_{dc} + e_n^-(E)] + c_n^0 \bar{p}^-_{dc}[\bar{n}^+_{dc} + e_p^+(E)]}{P^0(E)P^-(E) + N^+(E)P^-(E) + N^0(E)N^+(E)}\right] N^{DB}(E)dE \tag{16}$$

and

$$\frac{1}{\tau_p^{DB}} = \int_{E_v}^{E_c} \left[\frac{c_p^- \bar{n}^0_{dc}[\bar{n}^+_{dc} + e_p^+(E)] + c_p^0 \bar{n}^+_{dc}[\bar{p}^-_{dc} + e_n^-(E)]}{P^0(E)P^-(E) + N^+(E)P^-(E) + N^0(E)N^+(E)}\right] N^{DB}(E)dE\ . \tag{17}$$

The expressions of e_n^-, e_n^0, e_p^+, and e_p^0 as functions of the energy can be written from the results of Vaillant and Jousse[11] [see their Eqs. (18)]

$$e_n^-(E) = 2\bar{n}^0_{dc} \exp\left[-\frac{E_{Fn} - E - E_u}{k_B T}\right],$$
$$e_n^0(E) = \frac{\bar{n}^+_{dc}}{2} \exp\left[-\frac{E_{Fn} - E}{k_B T}\right] \tag{18}$$

and

$$e_p^+(E) = 2\bar{p}^0_{dc} \exp\left[\frac{E_{Fp} - E}{k_B T}\right],$$
$$e_p^0(E) = \frac{\bar{p}^-_{dc}}{2} \exp\left[\frac{E_{Fp} - E - E_u}{k_B T}\right]. \tag{19}$$

In the following we shall treat the two cases $E_u > 0$ and

$E_u > 0$, the semiconductor being under *steady-state quasiequilibrium* conditions. We shall assume that the capture rate of a carrier by a center bearing an opposite charge is higher than the capture rate of this carrier by a neutral center, so that $\bar{n}^0_{dc}\bar{p}^0_{dc}$ can be neglected compared to $\bar{n}^+_{dc}\bar{p}^-_{dc}$. For both $E_u > 0$ and $E_u < 0$, the detailed energy dependence of the occupation functions will be studied and simple expressions will be given for f^+_{dc}, f^0_{dc}, and f^-_{dc} as well as for τ_n^{DB} and τ_p^{DB}.

1. E_u positive

For energies above the dark equilibrium Fermi level E_F we have $e_p^+ \ll p^0_{dc}$ and $e_p^0 \ll p^-_{dc}$, and the expression of f^+_{dc} given by Eqs. (13) can be simplified into

$$f^+_{dc} = \frac{(\bar{p}^0_{dc} + e_n^0)(\bar{p}^-_{dc} + e_n^-)}{(\bar{p}^0_{dc} + \bar{n}^+_{dc} + e_n^0)(\bar{p}^-_{dc} + \bar{n}^0_{dc} + e_n^-)} . \tag{20}$$

From Eq. (20) we define two energy levels E^-_{tn} and E^0_{tn} by

$$e_n^-(E^-_{tn}) = \bar{n}^0_{dc} + \bar{p}^-_{dc}, \quad e_n^0(E^0_{tn}) = \bar{n}^+_{dc} + \bar{p}^0_{dc} . \tag{21}$$

In the same way, for energies lower than $E_F - E_u$ we have $e_n^- \ll n^0_{dc}$ and $e_n^0 \ll n^+_{dc}$, and we obtain the simplified expression for f^-_{dc},

$$f^-_{dc} = \frac{(\bar{n}^0_{dc} + e_p^0)(\bar{n}^+_{dc} + e_p^+)}{(\bar{p}^-_{dc} + \bar{n}^0_{dc} + e_p^0)(\bar{p}^0_{dc} + \bar{n}^+_{dc} + e_p^+)} , \tag{22}$$

from which we define two energy levels E^0_{tp} and E^+_{tp} by

$$e_p^+(E^+_{tp}) = \bar{p}^0_{dc} + \bar{n}^+_{dc}, \quad e_p^0(E^0_{tp}) = \bar{p}^-_{dc} + \bar{n}^0_{dc} . \tag{23}$$

By means of Eqs. (18) and (19) it can be easily shown that $E^0_{tn} - E^-_{tn} \approx E_u$ and $E^+_{tp} - E^0_{tp} \approx E_u$ within a few $k_B T$, and $E^0_{tn} \approx E_{Fn}$ if $n_{dc} \gg p_{dc}$ and $E^0_{tp} \approx E_{Fp} - E_u$ if $p_{dc} \gg n_{dc}$.

This approach of the statistics of the correlated states is quite close to the two-state model proposed by Halpern,[33] and it will be shown that, as far as the modulation of the photocurrent is concerned, we also obtain very similar results by taking into account either a single distribution of DB states or two distributions of monovalent states belonging to different species of traps.

We present in Fig. 2 the two different possibilities for the positions of E^-_{tn}, E^0_{tn}, E^0_{tp}, and E^+_{tp} within the gap of a semiconductor depending on whether $E^+_{tp} < E^-_{tn}$ or $E^-_{tn} < E^+_{tp}$. We have labeled the five intervals 1, 2, 3, 4, and 5 in the first case and 1, 2, 3′, 4, and 5 in the second one. Indeed, the intervals 1, 2, 4, and 5 are defined by the same inequalities in both cases as given in Appendix B. The occurrence of one situation or of the other depends on the semiconductor characteristics (in particular, the defect distribution), and, for a given semiconductor, also on the experimental conditions. The first situation (1,2,3,4,5) is likely to occur under high illumination and low temperature, while the second situation (1,2,3′,4,5) can be observed under low illumination and high temperature. To illustrate this, let us consider the case of intrinsic *a*-Si:H for which the dark Fermi level is located at say

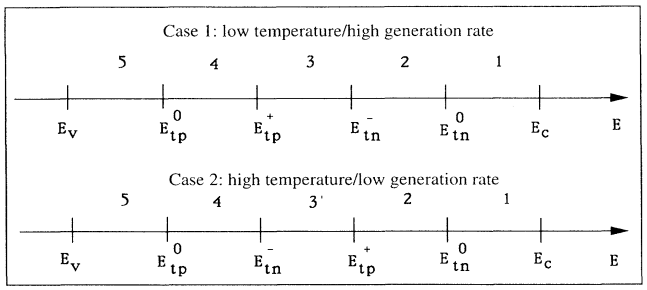

FIG. 2. Relative positions of E^-_{tn}, E^0_{tn}, E^0_{tp}, and E^+_{tp} within the gap of a semiconductor in the two different cases that can be encountered for positive values of the correlation energy. The case (1,2,3,4,5) corresponds to a steady-state quasiequilibrium far from dark equilibrium which can be observed for low temperatures and/or high generation rates. The case (1,2,3′,4,5) corresponds to a steady-state quasiequilibrium close to dark equilibrium, which can be observed for high temperatures and/or low generation rates.

0.75 eV below the conduction-band edge, as commonly found in the literature. At low temperature (e.g., 150 K) and high generation rate (e.g., 5×10^{18} cm^{-3}s^{-1}) the two quasi-Fermi-levels are well separated ($E_c - E_{Fn} \approx 0.4$ eV) and, a correlation energy of the order of 0.3 eV being assumed, we are likely to be in the first case. On the contrary, at high temperature (e.g., 400 K) and low generation rate (e.g., 5×10^{14} cm^{-3}s^{-1}) the two quasi-Fermi-levels are close to the dark Fermi level and thus we are likely to be in the second case.

Within each interval, simple energy-independent expressions can be obtained for the occupation functions of the DB states because it is possible to neglect some of the capture and emission rates in front of the others. The results are summarized in Table I. To confirm the validity of these simple approximate analytical expressions and to justify the choice of the energy limits defined by Eqs. (21) and (23), in Figs. 3(a) and 3(b) we present typical variations with the energy of the occupation functions in the first (1,2,3,4,5) and second (1,2,3′,4,5) cases, respectively. Each one of the five intervals is well distinct from the others in these figures. It is clear that the occupation functions can be considered as independent of the energy within each interval, and we have checked that their values are in perfect agreement with the analytical approximate expressions of Table I.

Depending on the values of n_{dc} and p_{dc}, some of the intervals may be hidden. In particular, the five regions are clearly visible in the second case only if the material is practically intrinsic and $n_{dc} \approx p_{dc}$. It is easily shown that in the case of an *n*-type or *p*-type material (even slightly *n* or *p*) then, according to the expressions of f^0_{dc}, only four different regions will be apparent. Indeed, $f^0_{dc} \approx 1$ in regions 2 and 3′ in an *n*-type material or $f^0_{dc} \approx 1$ in regions 3′ and 4 in a *p*-type material, so that regions 2 and 3′ or regions 3′ and 4 apparently merge into a single region for an *n*-type or *p*-type material, respectively.

To further illustrate this feature we present in Figs.

TABLE I. Simplified expressions of the occupation functions of the DB states in the different energy intervals in the gap for the two cases [(1,2,3,4,5) and (1,2,3',4,5)] that can exist if the correlation energy is positive, as described in Fig. 2.

Energy interval	1	2	3	or	3'	4	5
f_{dc}^{+}	1	$\frac{\bar{p}_{dc}^{0}}{\bar{p}_{dc}^{0}+\bar{n}_{dc}^{+}}$	$\frac{\bar{p}_{dc}^{0}\bar{p}_{dc}^{-}}{\bar{p}_{dc}^{0}\bar{p}_{dc}^{-}+\bar{n}_{dc}^{+}\bar{p}_{dc}^{-}+\bar{n}_{dc}^{+}\bar{n}_{dc}^{0}}$	or	0	0	0
f_{dc}^{0}	0	$\frac{\bar{n}_{dc}^{+}}{\bar{p}_{dc}^{0}+\bar{n}_{dc}^{+}}$	$\frac{\bar{n}_{dc}^{+}\bar{p}_{dc}^{-}}{\bar{p}_{dc}^{0}\bar{p}_{dc}^{-}+\bar{n}_{dc}^{+}\bar{p}_{dc}^{-}+\bar{n}_{dc}^{+}\bar{n}_{dc}^{0}}$	or	1	$\frac{\bar{p}_{dc}^{-}}{\bar{n}_{dc}^{0}+\bar{p}_{dc}^{-}}$	0
f_{dc}^{-}	0	0	$\frac{\bar{n}_{dc}^{+}\bar{n}_{dc}^{0}}{\bar{p}_{dc}^{0}\bar{p}_{dc}^{-}+\bar{n}_{dc}^{+}\bar{p}_{dc}^{-}+\bar{n}_{dc}^{+}\bar{n}_{dc}^{0}}$	or	0	$\frac{\bar{n}_{dc}^{0}}{\bar{n}_{dc}^{0}+\bar{p}_{dc}^{-}}$	1

4(a)–4(c) the evolution of the occupation functions with an increasing dc flux in a slightly n-type semiconductor. As mentioned above, only four regions can be seen in Fig. 4(b). Physically, we can put forward the evolution of the electron and hole populations to explain this point. Since the material is n type, a low dc flux results in a relative increase of p_{dc} much higher than that of n_{dc}. Therefore, E_{Fp} moves far from E_F but E_{Fn} remains close to E_F. This is why f_{dc}^{0} extends towards the valence band as soon as the "sample" is illuminated. At high flux, if the DOS is such that the populations of electrons and holes tend to equilibrate, we obtain the variations of the occupation functions as plotted in Fig. 4(c). Conversely, if the populations remain such that $n_{dc} \gg p_{dc}$, we obtain variations similar to those presented in Fig. 4(b). As a conclusion, if E_u is positive, the number of apparent regions wherein the occupation functions take constant approximate expressions is included between three, as for dark thermal equilibrium, and five.

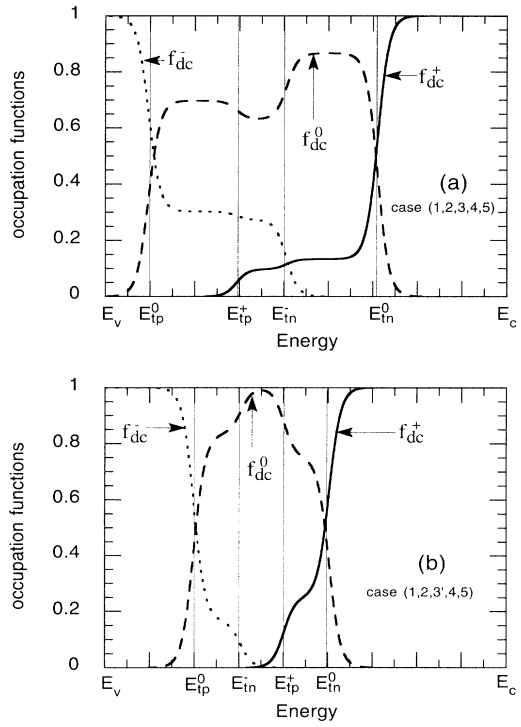

FIG. 3. Variations of the occupation functions f_{dc}^{+}, f_{dc}^{0}, and f_{dc}^{-} (full, dashed, and dotted lines, respectively) vs the energy in the two cases that can be encountered for positive values of the correlation energy E_u. The cases (1,2,3,4,5) and (1,2,3',4,5) are illustrated in (a) and (b), respectively. The parameters have been chosen so that the five different regions are clearly distinguishable in both cases. In both figures, the limits of the five regions are indicated as in Fig. 2.

Another interesting feature is presented in Fig. 5, namely the influence of the capture coefficients on the variations of the occupation functions. It can be seen that an increase of the capture coefficients of the *charged* centers results in an increase of the value of the *neutral* occupation function f_{dc}^{0}. Physically, this is due to the increase of the capture by charged centers of the carriers bearing the opposite charge. This capture transforms the charged dangling-bond centers (D^{-},D^{+}) into neutral ones (D^{0}). For instance, the increase of the capture coefficient c_n^{+} enhances the transition D^{+}+electron $\rightarrow D^{0}$, resulting in an increase of the density of D^{0} states.

From the above considerations it is interesting to derive simple expressions of the lifetimes associated to the DB centers, τ_n^{DB} for the electrons and τ_p^{DB} for the holes, as Taylor and Simmons[30] did for the monovalent states. If we assume that $n_{dc} \gg n_{dc0}$ and $p_{dc} \gg p_{dc0}$ and taking into account the expressions of the occupation functions derived above, one obtains from Eqs. (16) and (17)

$$\frac{1}{\tau_n^{DB}} = \int_{E_{tn}^{-}}^{E_{tn}^{0}} c_n^{+} f_{dc}^{+} N^{DB}(E)dE + \int_{E_{tp}^{0}}^{E_{tn}^{-}} (c_n^{+} f_{dc}^{+} + c_n^{0} f_{dc}^{0}) N^{DB}(E)dE \quad (24)$$

and

$$\frac{1}{\tau_p^{DB}} = \int_{E_{tp}^{+}}^{E_{tn}^{0}} (c_p^{-} f_{dc}^{-} + c_p^{0} f_{dc}^{0}) N^{DB}(E)dE + \int_{E_{tp}^{0}}^{E_{tp}^{+}} c_p^{-} f_{dc}^{-} N^{DB}(E)dE \quad (25)$$

in both (1,2,3,4,5) and (1,2,3',4,5) cases. Let us briefly comment on these equations, for instance, in the case

(1,2,3,4,5). In that case, taking the values ($=0$ or $\neq 0$) of the occupation functions into account, Eqs. (24) and (25) can be rewritten

$$\frac{1}{\tau_n^{\mathrm{DB}}} = \int_{E_{tn}^-}^{E_{tn}^0} c_n^+ f_{\mathrm{dc}}^+ N^{\mathrm{DB}}(E)dE + \int_{E_{tp}^+}^{E_{tn}^-} (c_n^+ f_{\mathrm{dc}}^+ + c_n^0 f_{\mathrm{dc}}^0) N^{\mathrm{DB}}(E)dE + \int_{E_{tp}^0}^{E_{tp}^+} c_n^0 f_{\mathrm{dc}}^0 N^{\mathrm{DB}}(E)dE \quad (26)$$

and

$$\frac{1}{\tau_p^{\mathrm{DB}}} = \int_{E_{tn}^-}^{E_{tn}^0} c_p^0 f_{\mathrm{dc}}^0 N^{\mathrm{DB}}(E)dE + \int_{E_{tp}^+}^{E_{tn}^-} (c_p^0 f_{\mathrm{dc}}^0 + c_p^- f_{\mathrm{dc}}^-) N^{\mathrm{DB}}(E)dE + \int_{E_{tp}^0}^{E_{tp}^+} c_p^- f_{\mathrm{dc}}^- N^{\mathrm{DB}}(E)dE \ , \quad (27)$$

respectively, the expressions of f_{dc}^0, f_{dc}^-, and f_{dc}^+ in each integral being those given in Table I in the corresponding energy interval.

According to Eqs. (23)–(27) we observe that the recombination via the DB centers only occurs between E_{tn}^0 and E_{tp}^0, and the states for which the energy is outside this interval act as traps for the carriers interacting with the nearest band. Furthermore, in that interval the recombination path can be divided into three components which are emphasized in Eqs. (26) and (27). Between E_{tn}^0 and E_{tn}^- the recombination occurs via the following process: $D^+ +$ electron $\rightarrow D^0$ and $D^0 +$ hole $\rightarrow D^+$. Consequently, the D^0 states act as traps for electrons via the process $D^0 +$ electron $\leftrightarrow D^-$, the electron being emitted

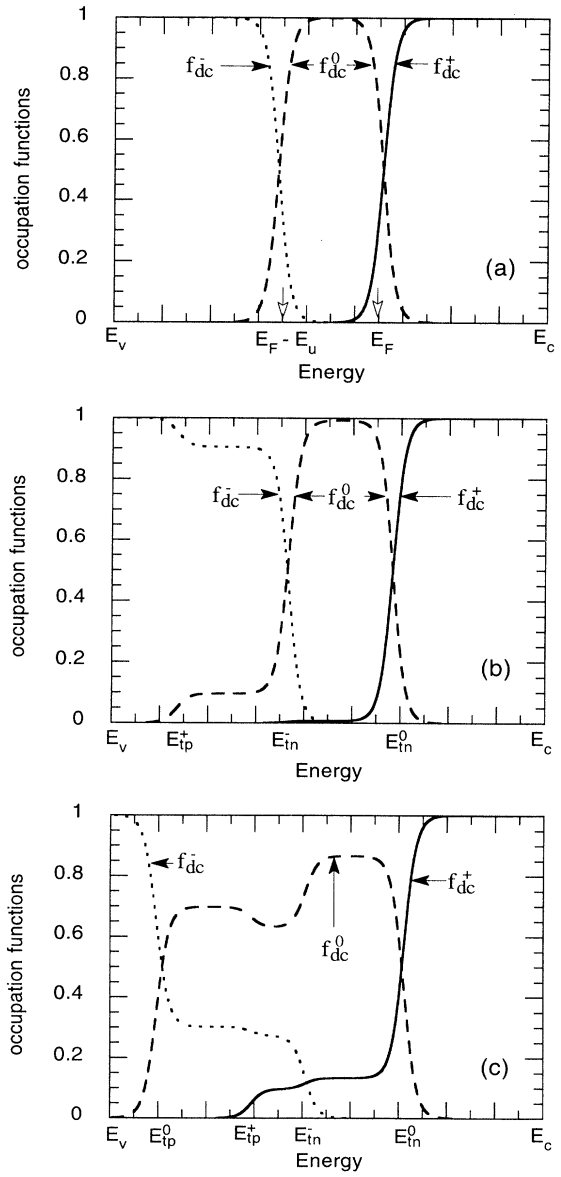

FIG. 4. Typical evolution of the variations of the occupation functions f_{dc}^+, f_{dc}^0, and f_{dc}^- (full, dashed, and dotted lines, respectively) vs the energy with increasing dc free-carrier densities in the case $E_u > 0$ for a slightly n-type semiconductor. In (a) the three regions corresponding to thermal equilibrium are recalled. In (b) the free-carrier densities have been slightly increased and a fourth region appears. In (c) the five different regions are visible because the steady-state conditions are far from thermal equilibrium and also because $n_{\mathrm{dc}} \approx p_{\mathrm{dc}}$.

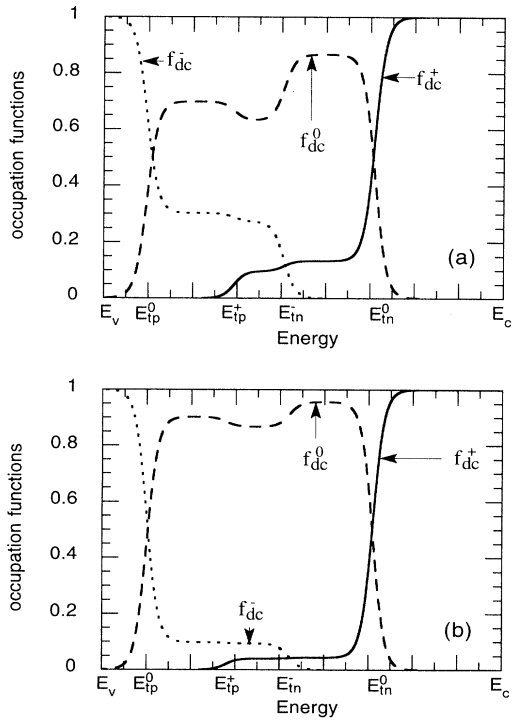

FIG. 5. Evolution of the variations of the occupation functions f_{dc}^+, f_{dc}^0, and f_{dc}^- (full, dashed, and dotted lines, respectively) vs the energy with increasing capture cross sections of the charged centers. An increase of the capture coefficients of the *charged* centers results in an increase of the occupation function of the *neutral* centers. This clearly appears if one compares the variations of the occupation functions in (a) with those of (b) for which the capture coefficients of the charged centers have been multiplied by a factor of 4.

from a D^- center towards the conduction band. Between E_{tp}^+ and E_{tp}^0 the recombination occurs via the following process: D^0+ electron $\rightarrow D^-$ and D^-+ hole $\rightarrow D^0$. Consequently, the D^0 states act as traps for holes via D^0+ hole $\leftrightarrow D^+$, the hole being emitted from a D^+ center towards the valence band. Finally, between E_{tn}^- and E_{tp}^+ both processes of recombination are involved, and all the states are recombining states. These behaviors are illustrated in Fig. 6 where the exchanges of carriers between the extended states and DB states are described as functions of the considered energy range. The same type of remarks and figure could be done for the case (1,2,3′,4,5) by changing the limits of the considered intervals.

Finally, it is worth pointing out that the expressions of the recombination lifetimes associated with a distribution of DB centers are not simply the integrals over the whole energy domain of the expressions derived by other authors for a single DB level. Indeed, for a single DB level, it was shown that the recombination lifetimes of electrons and of holes are respectively proportional to $c_n^+ f_{dc}^+ + c_n^0 f_{dc}^0$ and to $c_p^- f_{dc}^- + c_p^0 f_{dc}^0$.[18] Our calculation shows that $c_n^0 f_{dc}^0$ must not be taken into account between E_{tn}^- and E_{tn}^0, since there is no recombination path through the D^0/D^- transition in this interval. The same holds for $c_p^0 f_{dc}^0$ between E_{tp}^0 and E_{tp}^+, since there is no recombination through the D^+/D^0 transition in this interval.

2. E_u negative

The dissymmetry between the cases $E_u > 0$ and $E_u < 0$ already mentioned at equilibrium persists under steady-state conditions and the treatment of the occupation functions in the case $E_u < 0$ is different from that in the case $E_u > 0$. Taking into account that $E_u < 0$ in the expressions of the emission rates [Eqs. (18) and (19)], the denominator $D_f = P^0P^- + N^+P^- + N^0N^+$ of the occupation functions defined in Eqs. (13) can be simplified into

$$D_f = [e_n^0(\bar{p}_{dc}^- + e_n^-)] + [\bar{p}_{dc}^-\bar{p}_{dc}^0 + \bar{n}_{dc}^+\bar{p}_{dc}^- + \bar{n}_{dc}^+\bar{n}_{dc}^0] + [e_p^0(\bar{n}_{dc}^+ + e_p^+)] \, . \quad (28)$$

Typical variations of the bracketed quantities as functions of the energy are shown in Fig. 7(a). It appears clearly on the figure that, due to the exponential dependence upon energy of the emission rates, the main contribution to D_f comes from the third, second, and first quantities, respectively, as the energy increases from E_v to E_c. Therefore, we define two levels E_{tn} and E_{tp} by the following relations:

$$e_n^0(E_{tn})[e_n^-(E_{tn}) + \bar{p}_{dc}^-] = \bar{n}_{dc}^+[\bar{n}_{dc}^0 + \bar{p}_{dc}^-] + \bar{p}_{dc}^-\bar{p}_{dc}^0 \quad (29)$$

and

$$e_p^0(E_{tp})[e_p^+(E_{tp}) + \bar{n}_{dc}^+] = \bar{p}_{dc}^-[\bar{p}_{dc}^0 + \bar{n}_{dc}^+] + \bar{n}_{dc}^+\bar{n}_{dc}^0 \, , \quad (30)$$

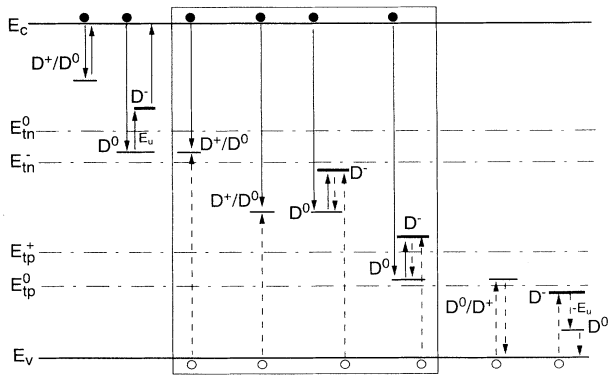

FIG. 6. Illustration of the exchanges of carriers between the extended states and the DB states for $E_u > 0$ in the case (1,2,3,4,5). Depending on the energy range considered, the DB states act as traps for carriers coming from the nearest band or as recombination centers. The traffic of the carriers between the extended states and the localized states is represented by arrows, the various recombination paths being put into a frame. Electrons are represented by full circles and holes by open circles.

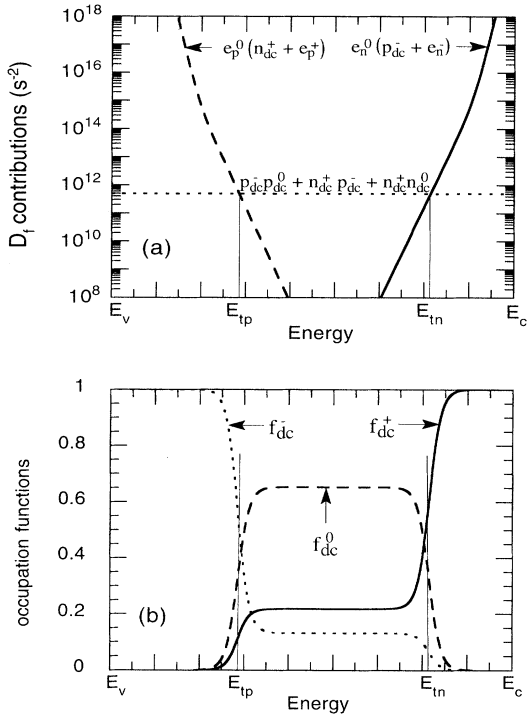

FIG. 7. In (a) the variations of three quantities are presented, the sum of which equals the denominator of the occupation functions for $E_u < 0$. One of this quantity (full lines) includes the emission rates of electrons towards the conduction band, the second one (dashed lines) the emission rates of holes towards the valence band, and the third one (dotted lines) only the capture rates of holes and electrons which are independent of the energy. The intersections of these curves define the two levels E_{tn} and E_{tp}. The corresponding variations of the occupation functions f_{dc}^+, f_{dc}^0, and f_{dc}^- (full, dashed, and dotted lines, respectively) are shown in (b), where these two levels clearly appear to play the role of quasi-Fermi-levels for trapped carriers for DB states with a negative correlation energy.

Eq. (30) being, as usual, the transformation by $\mathcal{T}$ of Eq. (29). Note that these levels are such that $E_{tn} > E_{Fn}$ and $E_{Fp} - E_u > E_{tp}$. According to the definitions of these levels it is possible to obtain simplified approximate expressions for the occupation functions in the energy intervals 1, 2, and 3 defined by $E > E_{tn}$, $E_{tp} < E < E_{tn}$, and $E < E_{tp}$, respectively. These expressions are independent of the energy within each of these intervals, and they are given in Table II. We present in Fig. 7(b) typical variations of the occupation functions in the case $E_u < 0$ using the same parameters as in Fig. 7(a). The three different ranges of energy are clearly distinguishable on the figure and compare perfectly well with the three regions observed in Fig. 7(a). Moreover, the occupation functions can be considered as independent of the energy within each of these ranges, and the constant values correspond to the expressions given in Table II.

As in the preceding subsection, taking the above results into account, we can derive the expressions of the lifetimes of electrons and holes associated to the DB states by means of Eqs. (16) and (17). We obtain

$$(\tau_n^{\mathrm{DB}})^{-1} = \int_{E_{tp}}^{E_{tn}} (c_n^+ f_{\mathrm{dc}}^+ + c_n^0 f_{\mathrm{dc}}^0) N^{\mathrm{DB}}(E) dE \tag{31}$$

and

$$(\tau_p^{\mathrm{DB}})^{-1} = \int_{E_{tp}}^{E_{tn}} (c_p^0 f_{\mathrm{dc}}^0 + c_p^- f_{\mathrm{dc}}^-) N^{\mathrm{DB}}(E) dE \ . \tag{32}$$

These relations show that the recombining states are only the states included between E_{tn} and E_{tp} and that the processes involved in the recombination are the following: $D^+ +$ electron $\rightarrow D^0$ and $D^0 +$ hole $\rightarrow D^+$ along with $D^0 +$ electron $\rightarrow D^-$ and $D^- +$ hole $\rightarrow D^0$. Outside this interval the states act as traps exchanging carriers with the nearest band. These behaviors are illustrated in Fig. 8 where the exchanges of carriers between the extended states and the DB centers are described depending as functions of the considered energy range.

It is worth noticing that our description of the occupation of the DB states works very well under steady-state conditions which are not too close to equilibrium conditions. Close to equilibrium, the peak located at $E_F - E_u/2$ that exists at equilibrium in the energy dependence of f_{dc}^0 still persists and its contribution has to be taken into account. This contribution increases with decreasing values of $|E_u|$. For instance, f_{dc}^0 has a maximum value equal to $\frac{1}{2}$ for $E_u = 0$. This means that the case of very low absolute values of the correlation energy, such as suggested by some authors in a-Si:H,[34] should require more refinements in the analysis to be perfectly described.

TABLE II. Simplified expressions of the occupation functions of the DB states in the different energy intervals of the gap if the correlation energy is negative. The labels 1, 2, and 3 correspond to $E > E_{tn}$, $E_{tn} > E > E_{tp}$, and $E_{tp} > E$, respectively.

Energy interval	1 $E > E_{tn}$	2 $E_{tn} > E > E_{tp}$	3 $E_{tp} > E$
f_{dc}^+	1	$\dfrac{\bar{p}_{\mathrm{dc}}^0 \bar{p}_{\mathrm{dc}}^-}{\bar{p}_{\mathrm{dc}}^0 \bar{p}_{\mathrm{dc}}^- + \bar{n}_{\mathrm{dc}}^+ \bar{p}_{\mathrm{dc}}^- + \bar{n}_{\mathrm{dc}}^+ \bar{n}_{\mathrm{dc}}^0}$	0
f_{dc}^0	0	$\dfrac{\bar{n}_{\mathrm{dc}}^+ \bar{p}_{\mathrm{dc}}^-}{\bar{p}_{\mathrm{dc}}^0 \bar{p}_{\mathrm{dc}}^- + \bar{n}_{\mathrm{dc}}^+ \bar{p}_{\mathrm{dc}}^- + \bar{n}_{\mathrm{dc}}^+ \bar{n}_{\mathrm{dc}}^0}$	0
f_{dc}^-	0	$\dfrac{\bar{n}_{\mathrm{dc}}^+ \bar{n}_{\mathrm{dc}}^0}{\bar{p}_{\mathrm{dc}}^0 \bar{p}_{\mathrm{dc}}^- + \bar{n}_{\mathrm{dc}}^+ \bar{p}_{\mathrm{dc}}^- + \bar{n}_{\mathrm{dc}}^+ \bar{n}_{\mathrm{dc}}^0}$	1

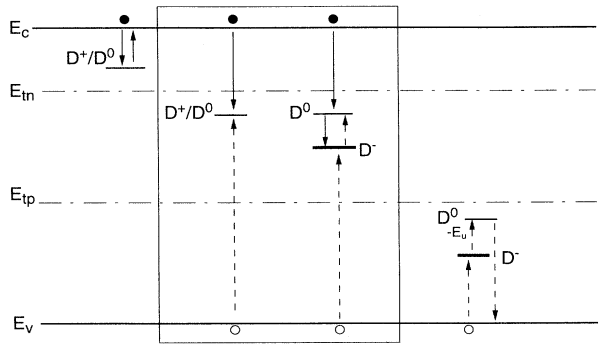

FIG. 8. Illustration of the exchanges of carriers between the extended states and the DB states for $E_u < 0$. Same symbols as in Fig. 6.

C. Study of the alternative contribution

If the expressions of the occupation functions given by Eqs. (13) and (14) are replaced into Eqs. (7) and (8), we obtain the following linear system of four equations:

$$\begin{aligned}
&A_n^{\mathrm{DB}} n_r - (B_n^{\mathrm{DB}} + \omega) n_i + A_p^{*\mathrm{DB}} p_r + B_p^{*\mathrm{DB}} p_i = G_{\mathrm{ac}} \ , \\
&(B_n^{\mathrm{DB}} + \omega) n_r + A_n^{\mathrm{DB}} n_i - B_p^{*\mathrm{DB}} p_r + A_p^{*\mathrm{DB}} p_i = 0 \ , \\
&A_n^{*\mathrm{DB}} n_r + B_n^{*\mathrm{DB}} n_i + A_p^{\mathrm{DB}} p_r - (B_p^{\mathrm{DB}} + \omega) p_i = G_{\mathrm{ac}} \ , \\
&B_n^{*\mathrm{DB}} n_r - A_n^{*\mathrm{DB}} n_i - (B_p^{\mathrm{DB}} + \omega) p_r - A_p^{\mathrm{DB}} p_i = 0 \ ,
\end{aligned} \tag{33}$$

where the expressions of the coefficients are given in Appendix C. If this linear system is solved for n_r, n_i, p_r, and p_i, the alternative contribution to the photocurrent is found from

$$I_{\mathrm{ac}} = Sq\xi[\mu_n n_r + \mu_p p_r + j(\mu_n n_i + \mu_p p_i)] \ . \tag{34}$$

Then, the phase shift Φ between the excitation and the modulated photocurrent as well as the modulus of this photocurrent such as $I_{\mathrm{ac}} = |I_{\mathrm{ac}}| \exp(-j\Phi)$ are given by

$$\tan(\Phi) = -\frac{\mu_n n_i + \mu_p p_i}{\mu_n n_r + \mu_p p_r} \ , \tag{35}$$

$$|I_{\mathrm{ac}}| = Sq\xi[(\mu_n n_i + \mu_p p_i)^2 + (\mu_n n_r + \mu_p p_r)^2]^{1/2} \ . \tag{36}$$

The system (33) stands only for a single type of correlated state, i.e., with energy-independent capture cross sections and a constant correlation energy E_u independent of the energy of the DB states. If other types of states are taken into account, then the coefficients of n_r, n_i, p_r, and p_i in the system (33) have to be changed by adding to the

present coefficients the equivalent coefficients corresponding to these other types of states (see Appendix C).

In the case $E_u > 0$ and considering the physics involved, it is clear that four specific levels, such that

$$e_n^-(E_{\omega n}^-) = e_n^0(E_{\omega n}^0) = e_p^0(E_{\omega p}^0) = e_p^+(E_{\omega p}^+) = \omega \ , \quad (37)$$

play an important role. Owing to the results of the preceding subsections it is easily understood that different cases will have to be taken into account depending on the relative positions of $E_{\omega n}^-$, $E_{\omega n}^0$, $E_{\omega p}^0$, and $E_{\omega p}^+$ compared with E_{tn}^-, E_{tn}^0, E_{tp}^0, and E_{tp}^+. In the following we shall treat separately the two cases:

(i) $\omega \ll \bar{n}_{\rm dc}^0 + \bar{p}_{\rm dc}^-$, $\omega \ll \bar{n}_{\rm dc}^+ + \bar{p}_{\rm dc}^0$;

(ii) $\omega \gg \bar{n}_{\rm dc}^0 + \bar{p}_{\rm dc}^-$, $\omega \gg \bar{n}_{\rm dc}^+ + \bar{p}_{\rm dc}^0$,

which define the recombination-limited regime and the trapping- and release-limited regime, respectively.

In the case $E_u < 0$ the definition of the specific emission levels $E_{\omega n}^-$, $E_{\omega n}^0$, $E_{\omega p}^0$, and $E_{\omega p}^+$ remains the same as for $E_u > 0$. Nevertheless, the precise determination of the two limiting regimes for the modulated photocurrent is not as simple as for $E_u > 0$. This is due to the intricate definitions of E_{tn} and E_{tp} where the products of different capture rates are involved.

From the study of the steady-state occupancy of the DB states, and as illustrated in Fig. 8, we know that all the DB states for which the D^0 level lies between E_{tn} and E_{tp} act as recombination centers, whatever their state of charge (D^0, D^-, or D^+). Moreover, we also know (see Table II) that above E_{tn} the DB centers are in the D^+ state, while for energies below E_{tp} they are in the D^- state. Thus we expect that the only capture and release processes which have to be taken into account are the following: (a) for the traffic with the conduction band, capture of an electron by a D^+ center located above E_{tn} to form a D^0 which then releases the electron to return in the D^+ state, (b) for the traffic with the valence band, capture of a hole by a D^- center below E_{tp} to form a D^0 which then releases the hole to return in the D^- state.

As a consequence, in the case $E_u < 0$ the release processes always occur from a neutral DB state. This means that among the four possible emission levels defined by Eq. (37), only the two levels $E_{\omega n}^0$ and $E_{\omega p}^0$ play an essential role, and the trapping and release regime is characterized by $E_{\omega n}^0 > E_{tn}$ and $E_{\omega p}^0 < E_{tp}$. In terms of the angular frequency ω, this can also be written $\omega \gg e_p^0(E_{tp})$ and $\omega \gg e_n^0(E_{tn})$. Using the definition of E_{tp} and E_{tn}, these two conditions can be explained by $\omega \gg \omega_p$ and $\omega \gg \omega_n$, where

$$\omega_p = \frac{\bar{p}_{\rm dc}^- \bar{n}_{\rm dc}^+}{8\bar{p}_{\rm dc}^0} \exp\left[-\frac{E_u}{k_B T}\right] \left\{ -1 + \left\{ 1 + 16 \frac{\bar{p}_{\rm dc}^0}{\bar{n}_{\rm dc}^+} \exp\left[\frac{E_u}{k_B T}\right] \left[\frac{\bar{n}_{\rm dc}^0}{\bar{p}_{\rm dc}^-} + \frac{\bar{p}_{\rm dc}^0}{\bar{n}_{\rm dc}^+} + 1 \right] \right\}^{1/2} \right\} , \quad (38)$$

the expression of ω_n being the transformation by $\mathcal{T}$ of the expression of ω_p. Thus the definition of the transition frequency in the case $E_u < 0$ is not simply related to the single capture rates as it is the case for $E_u > 0$. Simple relations can only be found if there is a strong predominant capture from one type of carriers. For instance, if $\bar{p}_{\rm dc}^- > \bar{p}_{\rm dc}^0 > (\bar{n}_{\rm dc}^+/4)\exp[-E_u/2k_BT] > \bar{n}_{\rm dc}^0$, the limits can be approximated by $\omega_p \approx (\bar{p}_{\rm dc}^-/2)\exp[-E_u/2k_BT]$ for the upper one and by $\omega_n \approx \bar{p}_{\rm dc}^0$ for the lower one. In a symmetrical case, if $\bar{n}_{\rm dc}^- > \bar{n}_{\rm dc}^0 > (\bar{p}_{\rm dc}^-/4)\exp[-E_u/2k_BT] > \bar{p}_{\rm dc}^0$, the limits can be approximated by $\omega_n \approx (\bar{n}_{\rm dc}^+/2)\exp[-E_u/2k_BT]$ for the upper one and by $\omega_p \approx \bar{n}_{\rm dc}^0$ for the lower one.

In summary, for $E_u < 0$, the low- and high-frequency regimes are defined, respectively, by (i) $\omega \ll \omega_n$ and $\omega \ll \omega_p$, and (ii) $\omega \gg \omega_n$ and $\omega \gg \omega_p$.

1. *Case (i): Low-frequency regime*

This case can be treated independently of the sign of the correlation energy assuming that ω verifies the conditions

$$\omega \ll \bar{n}_{\rm dc}^0 + \bar{p}_{\rm dc}^- , \quad \omega \ll \bar{n}_{\rm dc}^+ + \bar{p}_{\rm dc}^0 \quad \text{if } E_u > 0 ,$$

$$\omega \ll \omega_n , \quad \omega \ll \omega_p \quad \text{if } E_u < 0 .$$

Using the expressions of the coefficients of the system (33) given in Appendix C, it can be easily shown that, in a first-order approximation, $A_n^{\rm DB} = A_n^{*\rm DB}$ and $A_p^{\rm DB} = A_p^{*\rm DB}$. We then find the following expressions for $\tan(\Phi)$ and $|I_{\rm ac}|/\cos(\Phi)$:

$$\tan(\Phi) = -\frac{(B_p^{*\rm DB})(B_n^{*\rm DB}) - (B_p^{\rm DB}+\omega)(B_n^{\rm DB}+\omega)}{A_n^{\rm DB}(B_p^{*\rm DB}+B_p^{\rm DB}+\omega) + A_p^{\rm DB}(B_n^{*\rm DB}+B_n^{\rm DB}+\omega)} , \quad (39)$$

$$\frac{|I_{\rm ac}|}{\cos(\Phi)} = Sq\xi G_{\rm ac} \frac{\mu_n(B_p^{*\rm DB}+B_p^{\rm DB}+\omega) + \mu_p(B_n^{*\rm DB}+B_n^{\rm DB}+\omega)}{A_n^{\rm DB}(B_p^{*\rm DB}+B_p^{\rm DB}+\omega) + A_p^{\rm DB}(B_n^{*\rm DB}+B_n^{\rm DB}+\omega)} . \quad (40)$$

Looking at the frequency dependence of A_n^{DB}, B_n^{DB}, A_p^{DB}, B_p^{DB}, A_n^{*DB}, B_n^{*DB}, A_p^{*DB}, and B_p^{*DB}, it can be shown that $\tan(\Phi)$ varies linearly with ω whereas $|I_{ac}|/\cos(\Phi)$ is independent of ω.

Using stronger approximations for the coefficients, Eqs. (39) and (40) lead to the first-order approximate expressions

$$\Phi \approx 0 \tag{41}$$

and

$$|I_{ac}| = Sq\xi G_{ac}(\mu_n \tau_n^{DB} + \mu_p \tau_p^{DB}) . \tag{42}$$

As in the case of monovalent states,[28] we find that the same lifetimes are involved in the expressions of the modulus of the alternative part of the current and in that of its continuous part. In the case of DB states with a positive correlation energy, this shows that, if ω is such that $\omega \ll \bar{n}_{dc}^0 + \bar{p}_{dc}^-$ and $\omega \ll \bar{n}_{dc}^+ + \bar{p}_{dc}^0$, the ac photocurrent is mainly related to recombination-limited processes and its expression is similar to that of the dc one. In the case of DB states with a negative correlation energy the same remark applies for $\omega \ll \omega_p$ and $\omega \ll \omega_n$.

In summary, the interesting features of case (i) are the linear dependence of $\tan(\Phi)$ upon ω and the independence of $|I_{ac}|/\cos(\Phi)$ upon ω, as far as $\omega \ll \bar{n}_{dc}^0 + \bar{p}_{dc}^-$ and $\omega \ll \bar{n}_{dc}^+ + \bar{p}_{dc}^0$ if E_u is positive, or as far as $\omega \ll \omega_p$ and $\omega \ll \omega_n$ if E_u is negative. The consequences of these behaviors will be illustrated by means of the simulation in Sec. III.

2. *Case (ii): High-frequency regime*

This regime is defined by

$$\omega \gg \bar{n}_{dc}^0 + \bar{p}_{dc}^- , \quad \omega \gg \bar{n}_{dc}^+ + \bar{p}_{dc}^0 \quad \text{if } E_u > 0 ,$$
$$\omega \gg \omega_n , \quad \omega \gg \omega_p \quad \text{if } E_u < 0 .$$

In this regime, contrary to the low-frequency regime, the study has to be performed in different ways depending on whether the correlation energy is positive or negative.

(a) E_u positive. In the case $E_u > 0$ one finds that the only coefficients remaining in the system (33) are

$$A_n^{DB} = \frac{1}{\tau_n^{DB}} + \int_{E_{tn}^0}^{E_c} c_n^+ f_{dc}^+ \frac{\omega^2}{[e_n^0(E)]^2 + \omega^2} N^{DB}(E)dE + \int_{E_{tn}}^{E_{tn}^0} c_n^0 f_{dc}^0 \frac{\omega^2}{[e_n^-(E)]^2 + \omega^2} N^{DB}(E)dE , \tag{43}$$

$$B_n^{DB} = \int_{E_{tn}^0}^{E_c} c_n^+ f_{dc}^+ G_n^0(E) N^{DB}(E)dE + \int_{E_{tn}}^{E_{tn}^0} c_n^0 f_{dc}^0 G_n^-(E) N^{DB}(E)dE , \tag{44}$$

$$A_p^{DB} = \frac{1}{\tau_p^{DB}} + \int_{E_{tp}^0}^{E_{tp}^+} c_p^0 f_{dc}^0 \frac{\omega^2}{[e_p^+(E)]^2 + \omega^2} N^{DB}(E)dE + \int_{E_v}^{E_{tp}^0} c_p^- f_{dc}^- \frac{\omega^2}{[e_p^0(E)]^2 + \omega^2} N^{DB}(E)dE , \tag{45}$$

$$B_p^{DB} = \int_{E_{tp}^0}^{E_{tp}^+} c_p^0 f_{dc}^0 G_p^+(E) N^{DB}(E)dE + \int_{E_v}^{E_{tp}^0} c_p^- f_{dc}^- G_p^0(E) N^{DB}(E)dE , \tag{46}$$

where the values of f_{dc}^+, f_{dc}^0, and f_{dc}^- are those given in Table I and where the weighting functions $G_n^0(E)$, $G_n^-(E)$, $G_p^0(E)$, and $G_p^+(E)$ are given by

$$G_n^0(E) = \frac{\omega e_n^0(E)}{\omega^2 + e_n^0(E)^2} , \quad G_n^-(E) = \frac{\omega e_n^-(E)}{\omega^2 + e_n^-(E)^2} , \tag{47}$$

$$G_p^0(E) = \frac{\omega e_p^0(E)}{\omega^2 + e_p^0(E)^2} , \quad G_p^+(E) = \frac{\omega e_p^+(E)}{\omega^2 + e_p^+(E)^2} . \tag{48}$$

Equations (43)–(46) present some similarities with the expressions derived for the case of monovalent states in a previous paper,[28] except that, for the DB centers, two contributions describing the two possible interactions of free carriers with this kind of defect have to be taken into account. The weighting functions $G_n^0(E)$, $G_n^-(E)$, $G_p^0(E)$, and $G_p^+(E)$ are sharp peaked functions centered at $E_{\omega n}^-$, $E_{\omega n}^0$, $E_{\omega p}^0$, and $E_{\omega p}^+$, respectively. Therefore, B_n^{DB} and B_p^{DB} can be approximated by

$$B_n^{DB} = \frac{\pi}{2} k_B T \left[c_n^+ N^{DB}(E_{\omega n}^0) + c_n^0 \frac{\bar{n}_{dc}^+}{n_{dc}^+ + \bar{p}_{dc}^0} N^{DB}(E_{\omega n}^-) \right] , \tag{49}$$

$$B_p^{DB} = \frac{\pi}{2} k_B T \left[c_p^- N^{DB}(E_{\omega p}^0) + c_p^0 \frac{\bar{p}_{dc}^-}{\bar{p}_{dc}^- + \bar{n}_{dc}^0} N^{DB}(E_{\omega p}^+) \right] , \tag{50}$$

$E_{\omega n}^-$, $E_{\omega n}^0$, $E_{\omega p}^0$, and $E_{\omega p}^+$ being given by the relations

$$E_c - E_{\omega n}^- = k_B T \ln \left[\frac{2c_n^0 N_c}{\omega} \right] + E_u ,$$
$$E_c - E_{\omega n}^0 = k_B T \ln \left[\frac{c_n^+ N_c}{2\omega} \right] \tag{51}$$

and

$$E_{\omega p}^+ - E_v = k_B T \ln \left[\frac{2c_p^0 N_v}{\omega} \right] ,$$
$$E_{\omega p}^0 - E_v = k_B T \ln \left[\frac{c_p^- N_v}{2\omega} \right] - E_u . \tag{52}$$

A first consequence of the developments presented above is that, if the modulated photocurrent is mainly a current due to electrons, it is linked to the emission of electrons from states down to an energy located at E_u *below* the dark Fermi level. Indeed, at high temperature and low flux the quasi-Fermi-level for electrons is close to E_F. If ω is chosen so that $E_{\omega n}^0$ is slightly above E_F, then, except with extremely different capture coefficients (i.e., $c_n^0 \ll c_n^+$), $E_{\omega n}^-$ is located roughly at $E_F - E_u$. This means that even if the distribution of D^0 states is located *below* the dark Fermi level, the DB centers will be probed by

the modulated photocurrent experiment. This is absolutely *impossible* in the case of a monovalent distribution located at the same energy below E_F.

The other consequences of these developments can be illustrated by means of an example. Let us consider the case of an electron-controlled modulated photocurrent. Following the results presented elsewhere,[28] we obtain after simple calculations

$$c_n^+ N^{\mathrm{DB}}(E_{\omega n}^0)+c_n^0\frac{\bar{n}_{\mathrm{dc}}^+}{\bar{n}_{\mathrm{dc}}^+ +\bar{p}_{\mathrm{dc}}^0}N^{\mathrm{DB}}(E_{\omega n}^-) \approx \frac{2}{\pi k_B T}\left[\frac{G_{\mathrm{ac}}Sq\xi\mu_n \sin(\Phi)}{|I_{\mathrm{ac}}|}-\omega\right] . \quad (53)$$

This last relation shows that, as far as the modulated photocurrent is concerned, a single distribution of DB states behaves roughly as if two distributions of monovalent states belonging to two different trap species were taken into account: one distribution exchanging carriers between $E_{\omega n}^0$ and the conduction band with a capture coefficient equal to c_n^+, and another distribution exchanging carriers between $E_{\omega n}^-$ and the conduction band with a capture coefficient equal to $c_n^0 f_{\mathrm{dc}}^0(E_{\omega n}^-)$, which simplifies into c_n^0 if $n_{\mathrm{dc}} \gg p_{\mathrm{dc}}$. This is in agreement with the two-state model.[33] For high values of ω we have plotted in Fig. 9 the variations with the energy of the dimensionless quantity

$$b_n^{\mathrm{DB}}(E) = \frac{\{\beta_n^-(E)e_n^-(E)-\beta_n^+(E)\bar{n}_{\mathrm{dc}}^+ -\beta_n^0(E)[\bar{n}_{\mathrm{dc}}^0 - e_n^0(E)]\}}{c_n^+} , \quad (54)$$

which is the weighting factor of $N^{\mathrm{DB}}(E)$ in the integral of B_n^{DB} divided by c_n^+. The two peaks associated with the emission of electrons from $E_{\omega n}^0$ and $E_{\omega n}^-$ towards the conduction band are clearly distinguishable in the figure. In the same figure the variations of $b_p^{\mathrm{DB}}(E)$ are presented, that is, the weighting factor of $N^{\mathrm{DB}}(E)$ in the integral of B_p^{DB} divided by c_p^-. The expression of $b_p^{\mathrm{DB}}(E)$ is simply the transformation by $\mathcal{T}$ of Eq. (54). Two peaks associated with the emission of holes from $E_{\omega p}^0$ and $E_{\omega p}^+$ towards the valence band can also be seen.

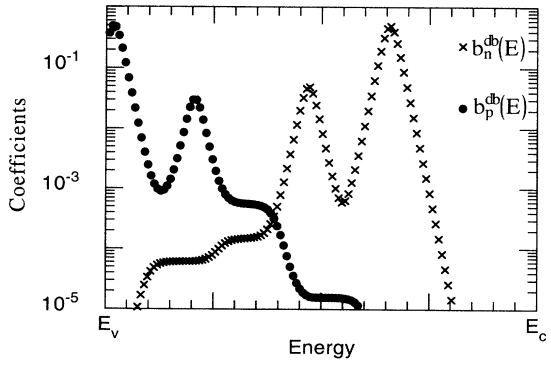

FIG. 9. Variations vs the energy of b_n^{DB} and b_p^{DB} (crosses and full circles, respectively) in the high-frequency regime for DB centers with a *positive* correlation energy. These quantities represent the weighting factors of $N^{\mathrm{DB}}(E)$ in the integrals of B_n^{DB} and B_p^{DB}, divided by c_n^+ and c_p^-, respectively. For both curves two peaks are observed, describing the emission of carriers from charged and neutral DB centers.

Equation (53) along with Eqs. (51) are simple relations connecting the density of DB states to the modulus and phase shift of the modulated photocurrent. They are the appropriate extensions to positively correlated DB states of the equations previously derived by Brüggemann *et al.* which are valid only for monovalent states.[26] Obviously, the same kind of relations could have been derived assuming that the modulated photocurrent is controlled by holes.

(b) E_u negative. In the case $E_u < 0$ the only remaining coefficients in the system (33) are

$$A_n^{\mathrm{DB}} = \frac{1}{\tau_n^{\mathrm{DB}}} + \int_{E_{tn}}^{E_c} c_n^+ \frac{\omega^2}{\omega^2+[e_n^0(E)]^2} N^{\mathrm{DB}}(E)dE , \quad (55)$$

$$B_n^{\mathrm{DB}} = \int_{E_{tn}}^{E_c} c_n^+ G_n^0(E) N^{\mathrm{DB}}(E)dE , \quad (56)$$

$$A_p^{\mathrm{DB}} = \frac{1}{\tau_p^{\mathrm{DB}}} + \int_{E_v}^{E_{tp}} c_p^- \frac{\omega^2}{\omega^2+[e_p^0(E)]^2} N^{\mathrm{DB}}(E)dE , \quad (57)$$

$$B_p^{\mathrm{DB}} = \int_{E_v}^{E_{tp}} c_p^- G_p^0(E) N^{\mathrm{DB}}(E)dE , \quad (58)$$

where the functions $G_n^0(E)$ and $G_p^0(E)$ are the same as in the case $E_u > 0$ and are given by Eqs. (47) and (48). Since the functions $G_n^0(E)$ and $G_p^0(E)$ are sharply peaked functions, B_n^{DB} and B_p^{DB} can be approximated by

$$B_n^{\mathrm{DB}} = \frac{\tau}{2} k_B T c_n^+ N^{\mathrm{DB}}(E_{\omega n}^0) , \quad (59)$$

$$B_p^{\mathrm{DB}} = \frac{\pi}{2} k_B T c_p^- N^{\mathrm{DB}}(E_{\omega p}^0) . \quad (60)$$

Equations (55)–(60) show that the results obtained for DB states with a negative correlation energy are very similar to those obtained for monovalent centers, taking into account the capture cross sections of the charged centers c_p^- and c_n^+ in place of c_p and c_n for monovalent states. As a consequence, as far as the modulated photocurrent is concerned, all the developments presented for monovalent states apply to the negatively correlated DB centers except that, in the case of a modulated photocurrent of holes, the correlation energy has to be taken into account for a proper energy scaling [see the expression of $E_{\omega p}^0$ in Eqs. (52)]. However, taking this particularity into account, it is possible to deduce the trap density shape from the equation proposed by Brüggemann *et al.*[26]

We present in Fig. 10 the variations of $b_p^{\mathrm{DB}}(E)$ and $b_n^{\mathrm{DB}}(E)$ for a high value of ω. As expected from our simplified expressions only a single peak appears for each function, as opposed to the case $E_u > 0$. From a physical point of view, the reason is that there are almost no neutral DB centers and the capture of free carriers occurs only via the charged centers.

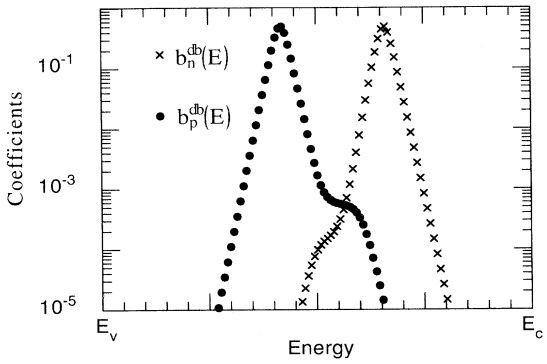

FIG. 10. Variations vs the energy of b_n^{DB} and b_p^{DB} (crosses and full circles, respectively) in the high-frequency regime for DB centers having a *negative* correlation energy. These quantities represent the weighting factors of $N^{DB}(E)$ in the integrals of B_n^{DB} and B_p^{DB}, divided by c_n^+ and c_p^-, respectively. On both curves a single peak is observed describing the emission of carriers from neutral DB centers only, as opposed to what is observed in Fig. 9 for a positive correlation energy.

III. SIMULATION

We do not intend to use our simulation to achieve a study as complete as in the case of monovalent states.[35] In regard to the results of the preceding section, most of the results presented in the case of monovalent states[28] can be translated immediately to the DB states. For instance, the development we made on the influence of the dc photon flux is still valid. Another important point is that the DOS is probed by the type of carriers which presents the highest $\mu/(N\sigma)$ factor, where μ is the free-carrier mobility, σ the capture cross section, and N the density of the trapping states for which the emission rate equals the angular frequency ω. We shall use this property in the following.

For a given distribution of defects (characterized by their position in the gap, their density of states, their capture cross sections, and their correlation energy in case of correlated states), and the equilibrium Fermi level E_{F0} at $T=0$ K being fixed, the following steps are performed in the simulation. First, the equilibrium Fermi level position is determined at each temperature (generally ranging from 150 to 450 K by 50-K steps) from the statement of charge neutrality and from the knowledge of E_{F0}. Thus we take account of a possible statistical shift of the Fermi level with the temperature as observed by different authors.[36,37] Then, the dc free-carrier densities n_{dc} and p_{dc} under illumination are obtained from the resolution of the continuity and neutrality relations [Eqs. (5), (6), and (9), respectively], taking account of the steady-state occupation of the DB states given by Eq. (13). Next, after calculation of the different coefficients A_n^{DB}, B_n^{DB}, A_p^{DB}, B_p^{DB}, A_n^{*DB}, B_n^{*DB}, A_p^{*DB}, and B_p^{*DB} taking all the types of states introduced in the gap into account (see the remark at the end of Appendix C), the real and imaginary parts of the ac components of the free carriers are calculated by solving the system (33) for each frequency of a set of 21 frequencies varying from $f_1=12$ Hz to $f_{21}=39.9$ kHz such that $f_{i+1}=1.5f_i$. Finally, the phase shift Φ and modulus $|I_{ac}|$ of the ac photocurrent are calculated from Eqs. (35) and (36).

We address successively the case of positive and negative correlation energies in Secs. III A and III B, respectively. In each case, we illustrate the characteristic features that can be linked to the DB states in the recombination-limited regime as well as in the trapping- and release-limited regime either when the DOS consists only of a single distribution of DB states or when the DOS consists of a distribution of DB states and distributions of monovalent band-tail states. Particular attention is paid to the transition between the two regimes and to the ability to deduce the trap distribution in the high-frequency regime by using simple analytical formulas which have been proved to be successful for the case of monovalent centers.

A. E_u positive

1. *Single distribution of DB states*

We choose a Gaussian distribution of DB states peaked at E_{DB} such that $E_c-E_{DB}=1$ eV with a maximum value of 10^{16} cm^{-3}eV^{-1} and a standard deviation $\sigma_{DB}=0.2$ eV. The correlation energy of the DB centers is taken equal to $E_u=0.3$ eV. The Fermi level at $T=0$ K cannot be chosen arbitrarily but has to be fixed at $E_{DB}+E_u/2$ to satisfy charge neutrality. The other parameters used for this simulation are the capture coefficients for the neutral states $c_n^0=c_p^0=2\times10^{-8}$ cm^{3}s^{-1}, the capture coefficients for the charged states $c_n^+=c_p^-=10\times c_n^0=2\times10^{-7}$ cm^{3}s^{-1}, the mobilities for electrons and holes $\mu_n=10$ cm^{2}V^{-1}s^{-1} and $\mu_p=1$ cm^{2}V^{-1}s^{-1}, respectively, the conduction cross-sectional area $S=4\times10^{-5}$ cm^2, the dc electric field $\xi=3000$ V cm^{-1}, and the equivalent densities of the conduction and valence bands $N_c=N_v=k_BTN_0$, with $N_0=10^{21}$ cm^{-3}eV^{-1}.

(a) Transition between the recombination-limited regime and the trapping- and release-limited regime. We first look at the transition between the two limiting regimes of the modulated photocurrent. We have shown in a previous paper that, in the case of a single species of monovalent traps, a simple evaluation of the capture cross section for the predominant type of carriers can be inferred from the threshold frequency corresponding to this transition. This threshold frequency can be obtained from a plot of $\cos(\Phi)/|I_{ac}|$ versus frequency. Indeed, in such a plot the recombination-limited regime corresponds to a plateau where $\cos(\Phi)/|I_{ac}|$ is constant, while in the trapping- and release-limited regime $\cos(\Phi)/|I_{ac}|$ increases with frequency and the curves corresponding to different light intensities gather at high frequency. We want to address this point when the DOS consists only of a Gaussian distribution of DB states in order to check if the frequencies involved in the transition between the two regimes are related to $\bar{n}_{dc}^0+\bar{p}_{dc}^-$ and $\bar{n}_{dc}^+ +\bar{p}_{dc}^0$, as suggested in the theoretical study in Sec. II C 1.

In Fig. 11(a) the frequency dependence of $\cos(\Phi)/|I_{ac}|$ at $T=400$ K for different values of the dc generation rate

is shown. A plateau is observed for the highest dc generation rates ($G_{dc} \geq 5\times10^{17}$ cm^{-3}s^{-1}). For the curve obtained with $G_{dc}=5\times10^{18}$ cm^{-3}s^{-1} the full and open arrows indicate the frequencies corresponding to the pulsations $\omega=\bar{n}^0_{dc}+\bar{p}^-_{dc}$ and $\omega=\bar{n}^+_{dc}+\bar{p}^0_{dc}$, respectively. It seems that the end of the plateau corresponds to $\bar{n}^0_{dc}+\bar{p}^-_{dc}$, which is always lower than $\bar{n}^+_{dc}+\bar{p}^0_{dc}$ in this case, the density of free electrons being always higher than the density of free holes as it could be expected from the Fermi-level position. This result is also confirmed by the dependence of tan(Φ) on frequency, shown on Fig. 11(b). Indeed, we observe that tan(Φ) varies linearly with frequency in the recombination regime for $\omega<\bar{n}^0_{dc}+\bar{p}^-_{dc}$ as predicted by the analytical approximations of Eq. (39).

In the case of Fig. 11, the ratios of the capture coefficients of the charged states to the capture coefficients of the neutral states are taken to be equal to 10. This is why the two possible frequencies for the transition are not well separated. To enlarge the interval between these two frequencies the ratios have been increased up to 500. The results are presented in Fig. 12. In Fig. 12(a) the frequency dependence of $\cos(\Phi)/|I_{ac}|$ obtained at $T=400$ K is shown. Note that, for all the dc generation rates we used, we observe a plateau, and consequently a recombination-limited regime, as opposed to the behavior of Fig. 11(a). This is due to the enhancement of the recombination linked to the increase of the D^0 contribution. Indeed, as shown in Fig. 5, an increase of the capture coefficients of the charged centers results in an increase of the value of f^0_{dc}. Therefore, since the recombination of carriers via the DB states always involves a D^0 center [see Eqs. (26) and (27)] the recombination is enhanced if the capture coefficients of the charged centers are increased.

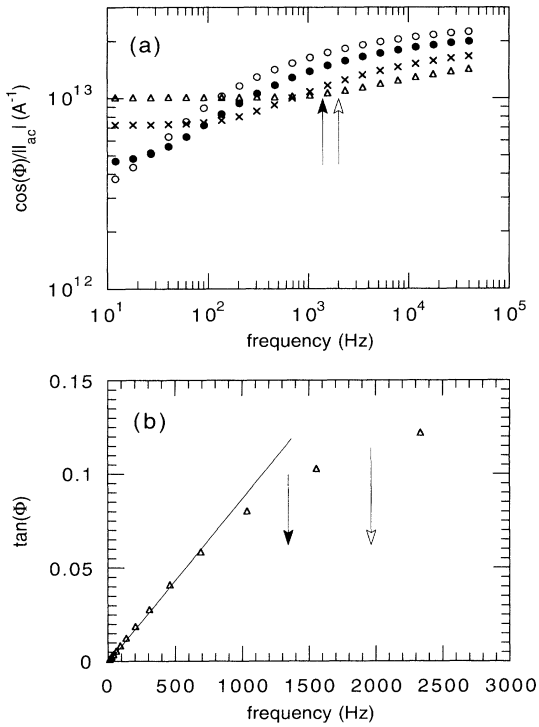

FIG. 11. Results of the simulation performed at $T=400$ K for a DOS consisting of a single Gaussian distribution of DB states such that $N(E)=N_{DB}\exp[-(E-E_{DB})^2/(2\sigma^2_{DB})]$ with $N_{DB}=10^{16}$ cm^{-3}eV^{-1}, $E_c-E_{DB}=1$ eV, $\sigma_{DB}=0.2$ eV, and a correlation energy $E_u=0.3$ eV. (a) Plots of $\cos(\Phi)/|I_{ac}|$ vs the modulation frequency under four different dc generation rates: (○) $G_{dc}=5\times10^{15}$ cm^{-3}s^{-1}; (●) $G_{dc}=5\times10^{16}$ cm^{-3}s^{-1}; (×) $G_{dc}=5\times10^{17}$ cm^{-3}s^{-1}; (△) $G_{dc}=5\times10^{18}$ cm^{-3}s^{-1}. All the curves are normalized to an ac generation rate $G_{ac}=5\times10^{13}$ cm^{-3}s^{-1}. On the curve corresponding to $G_{dc}=5\times10^{18}$ cm^{-3}s^{-1} we have indicated by a full arrow the frequency f_1 such that $2\pi f_1=\bar{n}^0_{dc}+\bar{p}^-_{dc}$ and by an open arrow the frequency f_2 such that $2\pi f_2=\bar{n}^+_{dc}+\bar{p}^0_{dc}$; (b) linear plot of tan(Φ) vs the frequency for $G_{dc}=5\times10^{18}$ cm^{-3}s^{-1}. The arrows of (a) are reported in (b). Both show that the end of the recombination-limited regime corresponds to f_1.

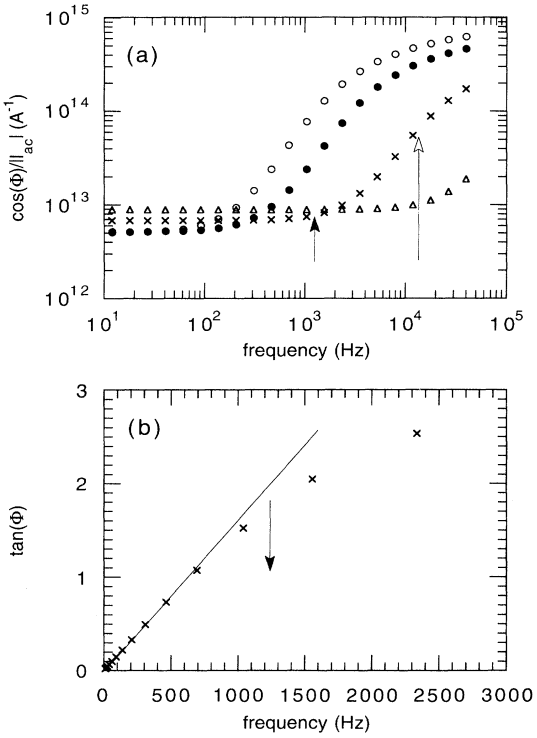

FIG. 12. The DOS of the studied "sample" being the same as for Fig. 11, the ratios of the capture cross sections of the charged DB centers to that of the neutral DB centers, c_n^+/c_n^0 and c_p^-/c_p^0, have been increased from 10 to 500. In (a) the plots of $\cos(\Phi)/|I_{ac}|$ vs the frequency are obtained from the results of our simulation performed at the same temperature and the same four different dc generation rates as for Fig. 11 (same symbols). All the curves are normalized to an ac generation rate $G_{ac}=5\times10^{13}$ cm^{-3}s^{-1}. On the curve obtained with $G_{dc}=5\times10^{17}$ cm^{3}s^{-1}, the full arrow indicates the frequency f_1 such that $2\pi f_1=\bar{n}^0_{dc}+\bar{p}^-_{dc}$ whereas the open arrow indicates the frequency f_2 for such that $2\pi f_2=\bar{n}^+_{dc}+\bar{p}^0_{dc}$. The end of the recombination-limited regime corresponds to f_1 as confirmed in (b) where tan(Φ) is linearly plotted vs the frequency. The frequency f_2 is out of the abscissa scale of this plot and the end of the linear variations of tan(Φ) clearly corresponds to f_1.

The arrows in Fig. 12(a) indicate the frequencies corresponding to the pulsations $\omega=\bar{n}_{dc}^{0}+\bar{p}_{dc}^{-}$ and $\omega=\bar{n}_{dc}^{+}+\bar{p}_{dc}^{0}$ for $G_{dc}=5\times10^{17}$ cm^{-3}s^{-1}. These two arrows are much better separated than in Fig. 11, and it is much clearer that the end of the plateau corresponds to $\bar{n}_{dc}^{0}+\bar{p}_{dc}^{-}$. Again, this is also confirmed by the linear plot of $\tan(\Phi)$ versus frequency shown in Fig. 12(b), where we observe that $\tan(\Phi)$ varies linearly with frequency in the recombination-limited regime for $\omega<\bar{n}_{dc}^{0}+\bar{p}_{dc}^{-}$.

In summary, if the DOS is made of a single distribution of DB centers with a positive correlation energy, it seems that the limit f_{lim} between the regime limited by recombination and the regime limited by trapping and release processes can be easily defined either from a plot of $\cos(\Phi)/|I_{ac}|$ versus frequency or from a linear plot of $\tan(\Phi)$ versus frequency. Moreover, if the electrons give the predominant contribution to both the dc current I_{dc} and the modulated photocurrent, then a good estimate of c_n^0/μ_n can be deduced from the measurement of I_{dc} and f_{lim}. If, in addition, the electron mobility μ_n is known, it is possible to obtain a good estimate of the electron-capture cross section σ_n^0 of the neutral DB centers. The same conclusions can be reached for σ_p^0 by considering that $2\pi f_{lim}=\bar{n}_{dc}^{+}+\bar{p}_{dc}^{0}\approx\bar{p}_{dc}^{0}$ if there is a strong predominant contribution of the holes.

It is worth noticing that the plots of $\cos(\Phi)/|I_{ac}|$ versus frequency presented in Figs. 11(a) and 12(a) behave in a way different from those obtained with a single species of monovalent states (see, for instance, Fig. 3 of Ref. 28). Indeed, whereas the curves obtained with a single species of monovalent centers under different generation rates converge towards the same curve for high modulation frequencies, the curves obtained with a single species of DB states cross one another. This behavior is a typical signature of the DB states. It is of great interest because it has been recently observed on *a*-Si:H samples, and it will be discussed in another paper where several experimental results obtained on *a*-Si:H will be presented.

(b) DOS reconstruction in the trapping- and release-limited regime. The calculated phase shift and modulus of the ac photocurrent are used to derive a DOS spectrum from the usual formulas[26,28]

$$N(E_\omega)=\frac{2}{\pi k_B T v\sigma}\left[\frac{Sq\mu\xi G_{ac}\sin(\Phi)}{|I_{ac}|}-\omega\right] \tag{61}$$

and

$$|E_{be}-E_\omega|=k_B T\ln\left[\frac{v\sigma k_B T N(E_{be})}{\omega}\right]. \tag{62}$$

We know that Eqs. (61) and (62) can be safely used for a single species of monovalent centers in the trapping- and release-limited regime which occurs at low illuminating intensities, provided there is a predominant contribution of one type of carrier to the modulated photocurrent. In this case, v, σ, and μ are, respectively, the thermal velocity, capture cross section, and mobility relative to the type of carriers that give the major contribution to the photocurrent, and E_{be} is the corresponding band edge. We want to test here the ability of such simple relations to reconstruct the DOS in case of the Gaussian distribution of DB states described above. To avoid a possible mixing of the contributions of both holes and electrons to the modulated photocurrent, we have decreased the mobility of the holes down to $\mu_p=0.1$ cm^{2}V^{-1}s^{-1}, keeping $\mu_n=10$ cm^{2}V^{-1}s^{-1}, so that the modulated photocurrent is determined by the electrons only. The other parameters are the same as described at the beginning of the present section, with $G_{dc}=5\times10^{15}$ cm^{-3}s^{-1} and the Fermi level E_{F0} at $T=0$ K such that $E_c-E_{F0}=0.85$ eV.

In Figs. 13(a) and 13(b) the results of the reconstruction by means of Eqs. (61) and (62) using $v\sigma=c_n^0$ and $v\sigma=c_n^+$, respectively, are shown (symbols). In Fig. 13(a) the result of the reconstruction after decreasing the energy determined from Eq. (62) by E_u (dashed lines) is also shown. In Figs. 13(a) and 13(b) the introduced DOS is drawn in full lines. Obviously, the reconstruction is imperfect. In Fig. 13(a) ($v\sigma=c_n^0$) good agreement is found

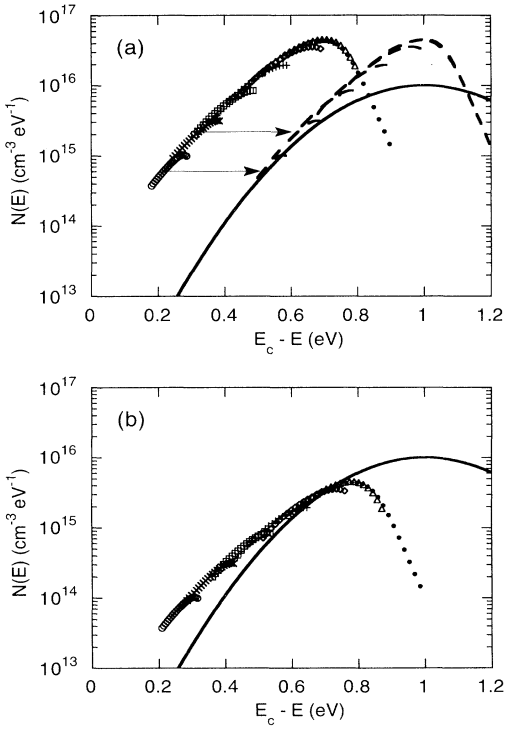

FIG. 13. The DOS introduced in the simulation (full line) consists of a Gaussian distribution of DB states peaked at E_{DB} such as $E_c-E_{DB}=1$ eV with a correlation energy $E_u=0.3$ eV. It is compared with the DOS reconstructed by means of the usual equations (61) and (62) (symbols). For the reconstruction, the capture coefficient used in both equations is (a) that of the D^0 center and (b) that of the D^+ center. The equilibrium Fermi level at $T=0$ K, E_{F0}, is such that $E_c-E_{F0}=0.85$ eV. Each set of symbols corresponds to a given temperature: (○) 150 K; (×) 200 K; (□) 250 K; (+) 300 K; (◇) 350 K; (△) 400 K; (●) 450 K and consists of 21 frequency points ranging from 12 Hz to 39.9 kHz. In (a) also shown by dashed lines is the result obtained after lowering the probed energy deduced from Eq. (62) by E_u. The DOS reconstruction is never perfect, due to the mixture coming from both D^0/D^- and D^+/D^0 transitions.

between the introduced DOS and the one reconstructed from the results of the simulation performed at *low* temperatures, taking into account a shift of the "probed" energy equal to E_u as predicted by the first equation of Eqs. (51). Conversely, in Fig. 13(b) ($v\sigma=c_n^+$) the best agreement is found with the results of the simulation performed at *high* temperatures without any shift of the probed energy according to the second equation of Eqs. (51). Note that the sharp drop observed mainly at the two highest temperatures is due to the transition from the trapping- and release-limited regime to the recombination-limited regime as extensively described in Ref. 28. At the intermediate temperatures, the shape of the DOS is only roughly reconstructed. The reason is that, when increasing the temperature, the major contribution to the modulated photocurrent shifts from capture and emission processes related to the D^0/D^- transition ($v\sigma=c_n^0$) to capture and emission processes related to the D^+/D^0 transition ($v\sigma=c_n^+$). This explains also why in Fig. 13(a) the values of the DOS reconstructed from the simulations performed for high temperatures are approximately ten times higher than the introduced DOS. Indeed, these data are plotted using $v\sigma=c_n^0$ instead of $v\sigma=c_n^+$ used in Fig. 13(b), the ratio c_n^+/c_n^0 being equal to 10.

This case is a clear illustration of the theoretical results obtained in Sec. II C 2, leading to Eq. (53), which emphasizes the mixture of the responses coming from both D^0/D^- and D^+/D^0 transitions. Another illustration will also be given below in the case of a more realistic DOS.

2. *More realistic DOS distribution*

One expects the DOS of amorphous semiconductors to consist of different kinds of states instead of a single Gaussian distribution of DB states. The shape of the DOS that will be used in the following consists of a Gaussian distribution of DB states and two band tails exponentially decreasing from the band edges toward midgap. This DOS is not representative of a special material but of an amorphous or glassy semiconductor in general. Indeed, the exponential band tails characterize the lack of long-range order in the material and should exist in any type of amorphous or glassy semiconductors,[1,2] while the DB states are typical deep gap states in these materials, with material-dependent parameters; for instance, in a-As_2Se_3, the DB states are believed to have negative correlation energies,[3] as opposed to a-Si:H where the DB states present a positive correlation energy.[6,38] As mentioned in the introduction of this section, the band-tail states are assumed to be monovalent,[1] as opposed to the DB states. Unless otherwise specified, the densities of states at the conduction- and valence-band edges have been fixed equal to 10^{21} $cm^{-3}eV^{-1}$. The slopes of the exponential distributions of the band-tail states are $1/(k_BT_c)$ and $-1/(k_BT_v)$ with $T_c=200$ K and $T_v=750$ K for the conduction- and valence-band tails, respectively. The distribution of DB states is represented by a Gaussian distribution as in Sec. III A 1, with a maximum equal to 10^{16} $cm^{-3}eV^{-1}$ and a standard deviation $\sigma_{DB}=0.05$ eV. The correlation energy E_u is equal to 0.3 eV. The capture coefficients $c_n^0=v_n\sigma_n^0$ and $c_p^0=v_p\sigma_p^0$ of the neutral dangling bonds have been taken independent of the temperature and equal to 2×10^{-8} cm^3s^{-1}. The same value has been taken for the capture coefficients c_n and c_p of the band-tail states. The capture coefficients of the charged dangling bonds c_p^- and c_n^+ are ten times larger ($c_p^-=c_n^+=2\times10^{-7}$ cm^3s^{-1}). The other parameters of the simulation are the same as above. The Fermi level at $T=0$ K is fixed at 0.85 eV below E_c. As shown in Fig. 14, two cases are considered, depending on the position E_{DB} of the maximum of the Gaussian DB states distribution: (a) $E_{DB}-E_v=1$ eV, so that $E_{F0}-E_u<E_{DB}<E_{F0}$; and (b) $E_{DB}-E_v=0.7$ eV, so that $E_{DB}>E_{F0}$. Also drawn in Fig. 14 are the DB states shifted by E_u, which are involved in the D^0/D^- transitions (dotted lines).

(a) Transition between the recombination-limited regime and the trapping- and release-limited regime. We present the plots of $\cos(\Phi)/|I_{ac}|$ as a function of the frequency obtained at $T=450$ K in Figs. 15(a) and 15(b) for the DOS of Figs. 14(a) and 14(b), respectively. Such a

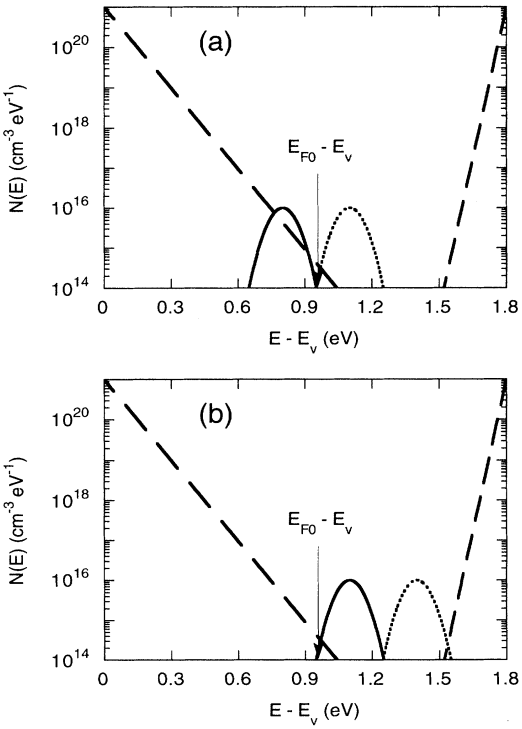

FIG. 14. Scheme of the DOS used in the following simulations, consisting of two exponential band-tail distributions (dashed lines) and a Gaussian distribution of DB states, the maximum of which is located at E_{DB} such that (a) $E_{DB}-E_v=0.8$ eV and (b) $E_{DB}-E_v=1.1$ eV. The states corresponding to the D^0/D^+ transition are represented by full lines and the states corresponding to the D^0/D^- transition are represented by dotted lines. The band-gap energy is $E_G=1.8$ eV and the Fermi level at $T=0$ K, E_{F0}, is located at 0.95 eV from E_v.

high temperature has been chosen to enhance the contribution of the deep gap states, i.e., the DB states, to the modulated photocurrent. We observe a quite different behavior in Figs. 15(a) and 15(b). On one hand, the results of Fig. 15(a) are comparable to what was observed in the study of a single species of monovalent traps (see, for instance, Fig. 3 of Ref. 28). On the other hand, in Fig. 15(b), the curves corresponding to different values of the dc generation rate cross each other, as already observed in Figs. 11 and 12. This feature is characteristic of the DB states and, more generally, traduces the ability of several species of traps having different capture cross sections to respond to the ac modulation simultaneously. The different behaviors of the curves in (a) and (b) are explained by the position of the DB states distribution. In Fig. 15(a), E_{DB} is *below* the Fermi level, but $E_{DB}+E_u$ is *above* the Fermi level. Thus, when interacting with the conduction band via the trapping and release of electrons, the Gaussian distribution of DB states behaves as a Gaussian distribution of a single species of monovalent

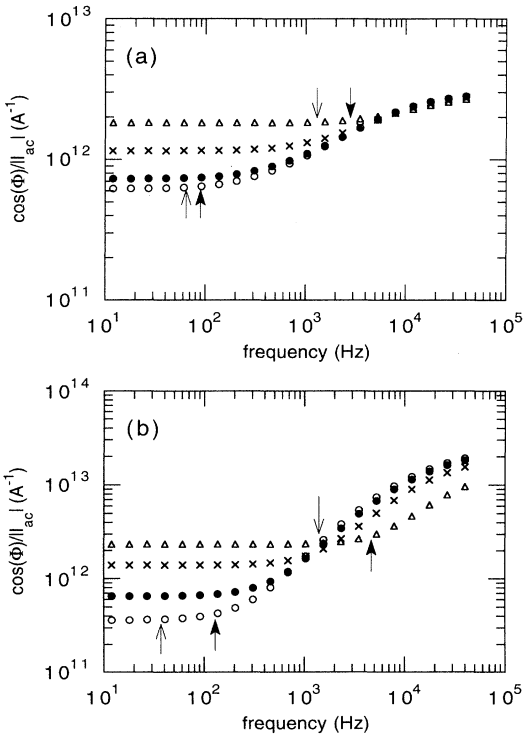

FIG. 15. Variations of $\cos(\Phi)/|I_{ac}|$ vs the frequency obtained at $T=450$ K with the DOS of Fig. 14, (a) with the DB distribution peaked at 0.8 eV above E_v and (b) with the DB distribution peaked at 1.1 eV above E_v. In both cases, the correlation energy of the DB centers is equal to 0.3 eV. The four sets of symbols correspond to four values of the dc generation rate G_{dc}: (○) 5×10^{15} cm^{-3}s^{-1}; (●) 5×10^{16} cm^{-3}s^{-1}; (×) 5×10^{17} cm^{-3}s^{-1}; (△) 5×10^{18} cm^{-3}s^{-1}. All the curves are normalized to an ac generation rate $G_{ac}=5\times10^{13}$ cm^{-3}s^{-1}. In both parts for the curves obtained with the lowest and highest dc generation rates, the full and simple arrows indicate the threshold frequencies corresponding to $2\pi f_{DB}=\bar{n}^0_{dc}+\bar{p}^-_{dc}$ and $2\pi f_{mono}=c_n n_{dc}+c_p p_{dc}$, respectively.

states located above E_F, at $E_{DB}+E_u$, corresponding to the D^0/D^- transition. Moreover, the electron-capture coefficient c_n^0 involved in this transition has been chosen to be identical to that of the states of the conduction-band tail. Therefore the contributions to the modulated photocurrent of the DB states and that of the conduction-band tail states appear as if these two different types of states belonged to the same species of traps. For this reason, there is no real mixing in the ac response coming from different species of traps and thus no crossing of the curves is observed. In Fig. 15(b), the peak of the DB states distribution is above the equilibrium Fermi level E_F, so that the two equivalent monovalent distributions of states corresponding to the capture of electrons by D^0 and D^+ states, which belong to different species owing to the different capture cross sections of charged and neutral DB centers, are located above E_F. Thus both can participate to the trapping and release traffic, and this leads to the crossing of the curves obtained under different dc generation rates.

To study the transition between the recombination-limited regime and the trapping- and release-limited regime we have indicated by full and simple arrows the frequencies f_{DB} and f_{mono} corresponding to the pulsation $\omega_{DB}=\bar{n}^0_{dc}+\bar{p}^-_{dc}$ and $\omega_{mono}=c_n n_{dc}+c_p p_{dc}$, respectively. From the discussion in Sec. II C, we know that ω_{DB} is the pulsation corresponding to the end of the recombination via the DB states in the present example while ω_{mono} corresponds to the end of the recombination via the band-tail states.[28] The arrows are put only on the curves obtained for the highest and the lowest dc generation rates in order to keep the figure clear enough.

It is quite unclear which arrow indicates the end of the plateau, that is, the end of the recombination-limited regime. Therefore, we have plotted in Figs. 16(a) and 16(b) the variations of $\tan(\Phi)$ versus frequency under the highest dc generation rate ($G_{dc}=5\times10^{18}$ cm^{-3}s^{-1}) for both (a) and (b) DOS cases, respectively. The arrows of Figs. 15(a) and 15(b) are reported in Figs. 16(a) and 16(b), respectively. In both figures it can be seen that the end of the recombination-limited regime corresponds to the lowest transition frequency, f_{mono} in the present case.

This shows that (i) if the plot of $\cos(\Phi)/|I_{ac}|$ is not always accurate for determining the end of the recombination-limited regime of the modulated photocurrent, the plot of $\tan(\Phi)$ versus frequency seems to give a better definition of the transition frequency; and (ii) from the plot of $\tan(\Phi)$ versus frequency one can deduce an order of magnitude of the lowest capture coefficient of all the states present in the gap of the studied semiconductor. This can be simply understood since the modulated photocurrent is fully limited by the recombination processes only when the frequency is lower than the lowest possible transition frequencies.

This last point has been confirmed by performing various simulations wherein the capture coefficients of the different distributions of states were taken very different from one another. The end of the linear dependence of $\tan(\Phi)$ upon frequency always gives an order of magnitude of the *lowest* transition frequency. As in the case of

a single distribution of DB centers, provided that the dc current is mainly due to one type of carrier, one can obtain an order of magnitude of the lowest capture coefficient.

(b) DOS reconstruction in the trapping- and release-limited regime. In Figs. 17(a) and 17(b) we present the results of the DOS reconstruction by means of Eqs. (61) and (62) in cases (a) and (b), respectively. Owing to the shape of the DOS and to the values of the free-carrier mobilities, the major contribution to the modulated photocurrent comes from the electrons ($N\sigma/\mu$ for electrons is always lower than $N\sigma/\mu$ for holes). Thus the reconstruction has been done using $\mu=\mu_n$ in both figures. Moreover, the $v\sigma$ product in Figs. 17(a) and 17(b) has been taken to be equal to that of the D^0 and D^+ centers, respectively, that is, $v\sigma=c_n^0=2\times10^{-8}$ cm^{3}s^{-1} in Fig. 17(a) and $v\sigma=c_n^+=2\times10^{-7}$ cm^{3}s^{-1} in Fig. 17(b). The original DOS is also shown on these figures (full lines for the DB states and dashed lines for the band-tail states). It is clearly seen that, in case (a) the DOS reconstruction leads to a *single* DOS bump representative of the DB distribution, the position of which is located E_u above $E_{\rm DB}$. On the contrary, we observe *two* well-defined DOS bumps in case (b), though there is only one Gaussian distribution of DB states. This is another good illustration of our calculation exposed in Sec. II C 2 (a). In Fig. 17(a), the position of the peak of the D^0 centers is below the Fermi level, so that no emission of electrons from the D^0 states toward the conduction band is observed, while, because of the *positive* correlation energy E_u, the position of the D^- states is above the Fermi level, enabling the emission of electrons from the D^- centers toward the conduction band to be observed. In Fig. 17(b), the deepest peak corresponds to the emission from the D^0 centers, which has been identified by the term $c_n^+N^{\rm DB}(E_{\omega n}^0)$ in Eq. (53). It is found with the proper energy position and density value compared with the DOS introduced in the simulation (shown in full lines in the figure), since the reconstruction has been performed with the parameter relative to the D^+/D^0 transition. In fact, the variations are somewhat smoothed and the reconstructed peak is found to be wider and with a peak amplitude lower than the introduced one; this is purely an effect of temperature dispersion which occurs if the DOS variations are sharp compared with $\exp(|E|/k_BT)$, as explained in Ref. 28. The other peak corresponds to the emission from the D^- centers and has been identified by the term $c_n^0 f_{\rm dc}^0(E_{\omega n}^-)N^{\rm DB}(E_{\omega n}^-)$ in Eq. (53); it is found at an energy approximately 0.3 eV ($=E_u$) closer to the conduction-band edge due to the difference between $E_{\omega n}^-$ and $E_{\omega n}^0$, as seen in Eqs. (51), and with an amplitude roughly reduced by a factor of 10 cor-

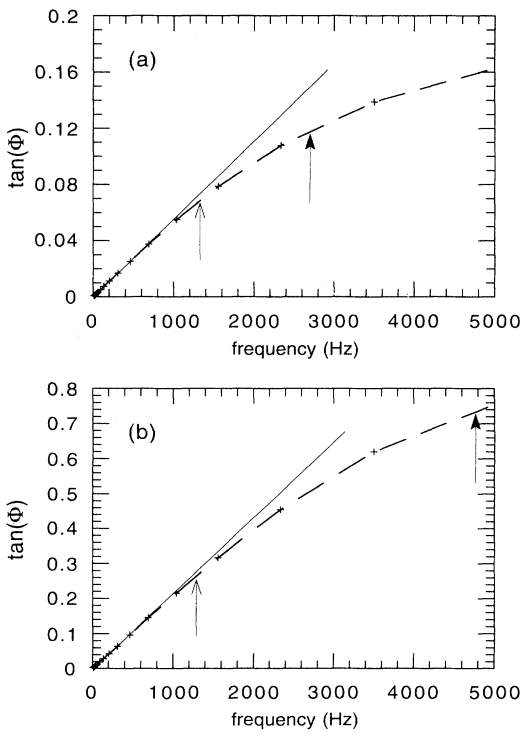

FIG. 16. Variations of tan(Φ) vs the frequency for $G_{\rm dc}=5\times10^{18}$ cm^{-3}s^{-1} in Figs. 15(a) and 15(b). On both parts, the full and simple arrows indicate the threshold frequencies corresponding to $2\pi f_{\rm DB}=\bar{n}_{\rm dc}^0+\bar{p}_{\rm dc}^-$ and $2\pi f_{\rm mono}=c_n n_{\rm dc}+c_p p_{\rm dc}$, respectively. The end of the linear variations of tan(Φ) clearly corresponds to $c_n n_{\rm dc}+c_p p_{\rm dc}$, which is lower than $\bar{n}_{\rm dc}^0+\bar{p}_{\rm dc}^-$.

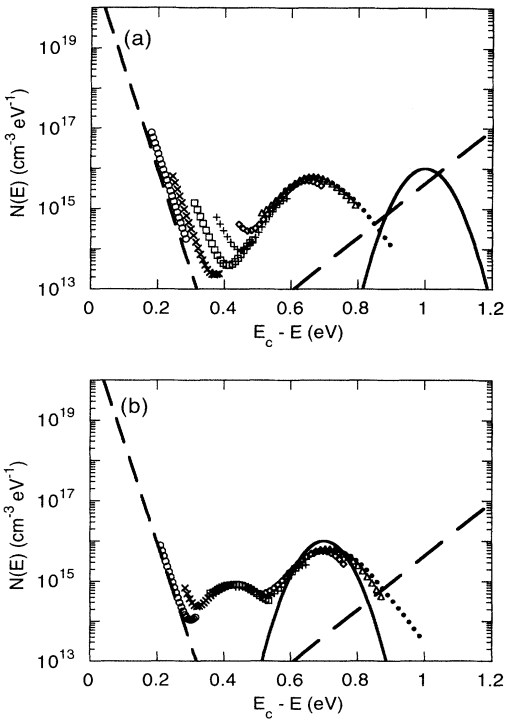

FIG. 17. The DOS introduced in the simulation (full line for the DB states and dashed lines for the band tails) is compared with the DOS reconstructed by means of Eqs. (61) and (62) (same symbols as for Fig. 13) for a Gaussian distribution of DB states peaked at $E_{\rm DB}$ such that (a) $E_c-E_{\rm DB}=1$ eV and (b) $E_c-E_{\rm DB}=0.7$ eV. The correlation energy is $E_u=0.3$ eV. The equilibrium Fermi level E_{F0} at $T=0$ K is such that $E_c-E_{F0}=0.85$ eV. The reconstructed DOS is calculated using (a) $v\sigma=c_n^0$ and (b) $v\sigma=c_n^+$.

responding to the ratio f_n^+/c_n^0 of the capture coefficient of positively charged DB centers to that of neutral DB centers.

Figures 17(a) and 17(b) clearly emphasize the role of the correlation energy. Indeed, as far as the states located between E_F and E_F-E_u are concerned, no response of the monovalent valence-band tail states is observed, though their density is comparable to that of the DB states for energies around 1 eV below E_c where both distributions overlap [see Fig. 17(a)]. This shows that the DB states can be probed even if located below E_F. Nevertheless, if the position of the DB states distribution falls below E_F-E_u, then no emission of electrons towards the conduction band can be seen, and the presence of DB centers cannot be detected from their interactions with the conduction band.

Symmetrically, if the dominant contribution to the modulated photocurrent comes from the holes instead of the electrons, then the signature of a distribution of DB states peaked at E_{DB} can consist of either two or a single bump in the reconstructed DOS, whether E_{DB} lies below E_F-E_u or between E_F-E_u and E_F. No signature is observed if E_{DB} is above E_F.

The results of Figs. 15–17 are easily interpreted in the framework of the developments which have been done for the monovalent centers,[28] if one considers that a distribution of DB states peaked at E_{DB} is equivalent to two distributions of monovalent centers peaked at E_{DB} and $E_{DB}+E_u$, respectively, with capture coefficients equal to those involved in the D^+/D^0 and D^0/D^- transitions, respectively. To emphasize the equivalence between the behavior of the DB centers and the two-state model,[33] we present in Fig. 18 the curves of $\cos(\Phi)/|I_{ac}|$ as a function of frequency obtained at a dc generation rate

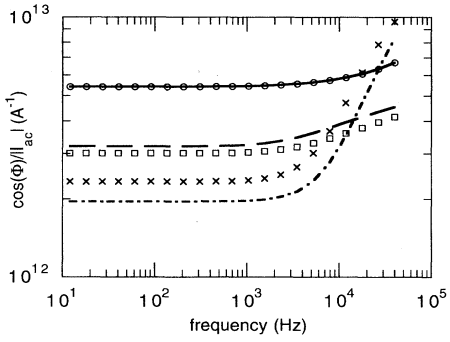

FIG. 18. Frequency dependence of $\cos(\Phi)/|I_{ac}|$ obtained under a dc generation rate $G_{dc}=5\times10^{18}$ cm^{-3}s^{-1} for the DOS of Fig. 14(b) where a Gaussian distribution of DB states is centered at $E_{DB}-E_v=1.1$ eV. The results are shown for three temperatures: 150 K (○), 300 K (□), and 450 K (×). These results are compared with those obtained if the Gaussian distribution of DB states is replaced by two Gaussian distributions of monovalent states centered at E_{DB} and $E_{DB}+E_u$, with the capture cross sections involved in the D^+/D^0 and D^0/D^- transitions, respectively. The solid line, dashed line, and dash-dotted line correspond to temperatures equal to 150, 300, and 450 K, respectively.

$G_{dc}=5\times10^{18}$ cm^{-3}s^{-1} and at three temperatures (150, 300, and 450 K) for two different kinds of DOS. The first DOS is that of Fig. 14(b) where a single Gaussian distribution of DB states is centered at $E_c-E_{DB}=0.7$ eV. In the second DOS the Gaussian distribution of DB states has been replaced by two identical Gaussian distributions (i.e., same values for the maximum and the standard deviation) of monovalent centers. The first distribution of monovalent traps is centered at E_{DB}, the states having capture coefficients for electrons and holes equal to c_n^+ and c_p^0, respectively. The second distribution of monovalent states is centered at $E_{DB}+E_u$, the states having capture coefficients for electrons and holes equal to c_n^0 and c_p^-, respectively. It is clear from Fig. 18 that the results obtained for a single distribution of DB states (symbols) compare well with the results obtained for two distributions of monovalent centers (lines) in the whole ranges of temperature and frequency.

B. E_u negative

In this part we follow the same presentation as for $E_u>0$. Thus we first focus on the case where the DOS consists of a Gaussian distribution of DB states only, before looking at the case where band-tail states are also taken into account. In each subsection, we address both the issue of the determination of the transition between the recombination-limited and trapping- and release-limited regimes, and that of the DOS reconstruction.

1. Single distribution of DB states

We consider a single Gaussian distribution of DB states peaked at E_{DB} such that $E_c-E_{DB}=0.8$ eV with a maximum value of 10^{16} cm^{-3}eV^{-1} and a standard deviation $\sigma_{DB}=0.2$ eV. The correlation energy of the DB centers is chosen to be equal to $E_u=-0.3$ eV. The Fermi level E_{F0} at $T=0$ K cannot be chosen arbitrarily but has to be fixed at $E_{DB}+E_u/2$ for the charge neutrality to be satisfied.

(a) Transition between the recombination-limited regime and the trapping- and release-limited regime. In Fig. 19 we present the plots of $\cos(\Phi)/|I_{ac}|$ versus the frequency obtained from the results of simulations performed at $T=400$ K under four different generation rates ranging from 5×10^{15} to 5×10^{18} cm^{-3}s^{-1} in two cases: (a) $\mu_n=10$ cm^{2}V^{-1}s^{-1} and $\mu_p=0.1$ cm^{2}V^{-1}s^{-1}, and (b) $\mu_n=0.1$ cm^{2}V^{-1}s^{-1} and $\mu_p=10$ cm^{2}V^{-1}s^{-1}.

In case (a) the modulated photocurrent is determined by the electrons whereas in case (b) it is determined by the holes. We first note that we observe a plateau for all the curves, and that the curves are crossing each other, as in the case of a positive E_u. From the analysis of Sec. II C, the threshold frequency should correspond to the lowest of ω_p and ω_n, the expressions of which are given, respectively, by Eq. (38) and by its transformation by $\mathcal{T}$. According to these expressions, ω_p and ω_n are independent of the mobility values. For the lowest and highest

generation rates ($G_{dc}=5\times10^{15}$ and 5×10^{18} $cm^{-3}s^{-1}$, respectively), we have indicated by a full arrow the frequency f_p given by $2\pi f_p=\omega_p$ and by an open arrow the frequency f_n given by $2\pi f_n=\omega_n$. Since they do not depend on the mobility values, the full and open arrows in Fig. 18(a) are at the same position as in Fig. 18(b). Actually, the threshold frequency clearly corresponds to the lowest of f_n and f_p in both cases (a) and (b) for $G_{dc}=5\times10^{18}$ $cm^{-3}s^{-1}$. This can also be seen in Fig. 20, which shows that the dependence of tan(Φ) on frequency is linear for frequencies below f_n. But for $G_{dc}=5\times10^{15}$ $cm^{-3}s^{-1}$, the transition in case (b) seems to occur at an intermediate value between f_n and f_p. The discrepancy between f_n and the end of the linear dependence of tan(Φ) upon frequency can also be seen in Fig. 21. Actually, for such a low generation rate, the steady-state thermodynamical conditions are very close to those of dark equilibrium. This is the origin of the observed discrepancies. Indeed, our analysis in the case of negative correlation energies is expected to give accurate results only if the steady-state

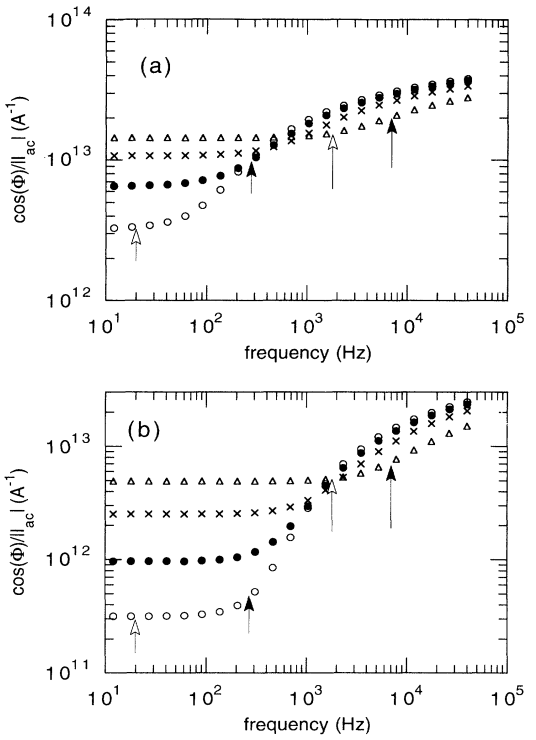

FIG. 19. Frequency dependence of $\cos(\Phi)/|I_{ac}|$ obtained at $T=400$ K for the DOS consisting of a single DB distribution peaked at 0.8 eV below E_c, a standard deviation $\sigma_{DB}=0.2$ eV, and a correlation energy equal to -0.3 eV for two couples of carrier mobilities: (a) $\mu_n=10$ $cm^2V^{-1}s^{-1}$ and $\mu_p=0.1$ $cm^2V^{-1}s^{-1}$ and (b) $\mu_n=0.1$ $cm^2V^{-1}s^{-1}$ and $\mu_p=0.1$ $cm^2V^{-1}s^{-1}$. (Same symbols as in Fig. 15.) All the curves are normalized to an ac generation rate $G_{ac}=5\times10^{13}$ $cm^{-3}s^{-1}$. In both parts, for the curves obtained with the lowest and the highest dc generation rates, the full arrows and the open arrows indicate the transition frequencies in the modulated photocurrent corresponding, respectively, to ω_p and ω_n, defined by Eq. (38).

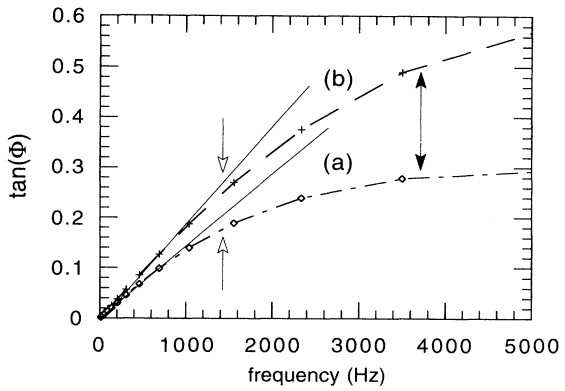

FIG. 20. Linear plot of tan(Φ) vs the modulation frequency for $G_{dc}=5\times10^{18}$ $cm^{-3}s^{-1}$ at $T=400$ K for the two cases considered in Fig. 19, ($\Diamond$) and (+) for cases (a) and (b), respectively. The full and open arrows indicate the threshold frequencies corresponding, respectively, to ω_p and ω_n, defined by Eq. (38), which are the same in (a) and (b). The full lines are extrapolations of the linear dependence of tan(Φ) upon frequency observed at low frequencies. The end of the linear dependence of tan(Φ) upon frequency corresponds to the lowest of ω_n and ω_p, which is here equal to ω_n.

conditions are far enough from equilibrium. In particular, the distribution of the D^0 centers is not well reproduced for thermodynamical conditions close to equilibrium, and more refinements would be needed to better explain all the behaviors in this regime.

(b) DOS reconstruction in the trapping- and release-limited regime. In Figs. 22(a) and 22(b) the results of the

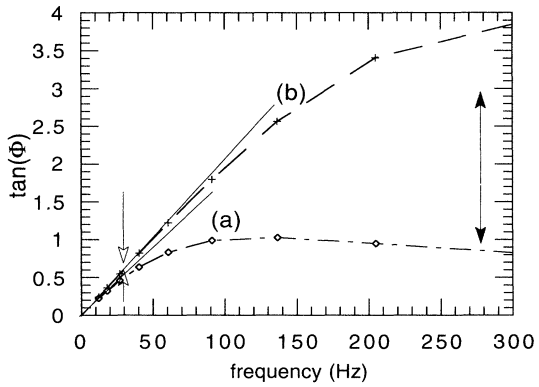

FIG. 21. Linear plot of tan(Φ) vs the modulation frequency for $G_{dc}=5\times10^{15}$ $cm^{-3}s^{-1}$ at $T=400$ K for the two cases considered in Fig. 19, ($\Diamond$) and (+) for cases (a) and (b), respectively. The full and open arrows indicate the threshold frequencies corresponding, respectively, to ω_p and ω_n, defined by Eq. (38), which are the same in (a) and (b). The full lines are extrapolations of the linear dependence of tan(Φ) upon frequency observed at low frequencies. This linear dependence does not end for the same frequencies in both cases; indeed, the agreement is quite good for case (a) where the threshold corresponds to ω_n, but in case (b), the threshold seems to correspond neither to ω_n nor to ω_p, but rather to an intermediate value.

reconstruction by means of Eqs. (61) and (62) using $v\sigma=c_n^+$, $\mu=\mu_n$, and $v\sigma=c_p^-$, $\mu=\mu_p$, respectively, are shown. Indeed, in cases (a) and (b) the modulated photocurrent is determined by the electrons and holes, respectively. The agreement between the DOS reconstructed (symbols) and that introduced in the simulation (full lines) is very good in case (a), where the DB centers are detected via the emission of *electrons* from the D^0 centers. In case (b) the DOS reconstruction is good if the "probed" energy is increased by $|E_u|$, as shown by dashed lines in Fig. 22(b). This emphasizes that if the modulated photocurrent is controlled by the *holes*, the negatively correlated DB centers are detected via the emission of *holes* from the D^0 centers. Since the corresponding emission rate involves the correlation energy as can be seen in Eqs. (52), one has to subtract it from the probed energy calculated from Eq. (62) to obtain the proper energy location of the DB centers in the gap.

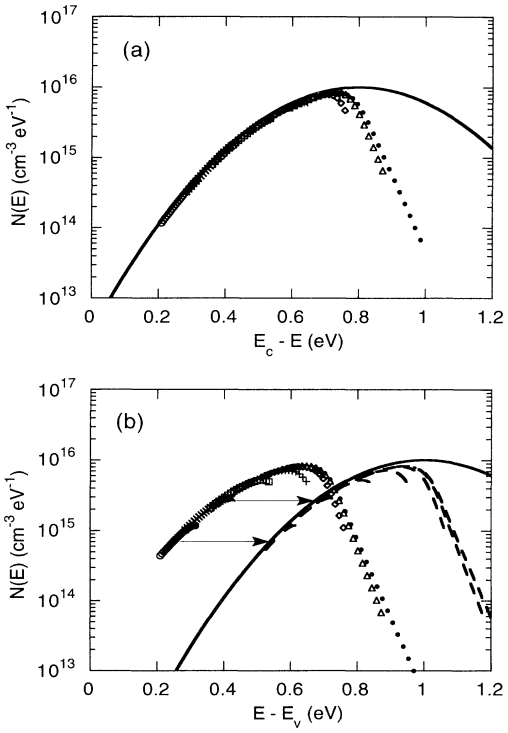

FIG. 22. The DOS reconstructed by means of Eqs. (61) and (62) (same symbols as in Fig. 13) is compared with the DOS introduced in the simulation (full line) which corresponds to a Gaussian distribution of DB states peaked at E_{DB} such that $E_c-E_{DB}=0.8$ eV, in two cases: (a) $\mu_n=10$ cm^{2}V^{-1}s^{-1}, $\mu_p=0.1$ cm^{2}V^{-1}s^{-1} and (b) $\mu_n=0.1$ cm^{2}V^{-1}s^{-1}, $\mu_p=10$ cm^{2}V^{-1}s^{-1}. The correlation energy is $E_u=-0.3$ eV. The reconstructed DOS is calculated using (a) $v\sigma=c_n^+$ and (b) $v\sigma=c_n^-$ and $\mu=\mu_p$. The reconstruction is very good in (a). In (b) the results obtained after increasing the probed energy deduced from Eq. (62) by $|E_u|$ are also shown by dashed lines. Then, the reconstruction is also very good.

2. *Gaussian distribution of DB states with two exponential band-tail states distributions*

We consider a DOS consisting of two exponential distributions of band-tail states and a Gaussian distribution of DB states. The characteristics of the band tails are the same as in Sec. III A 2. The Gaussian distribution of DB states is peaked at E_{DB} such that $E_c-E_{DB}=0.6$ eV with a maximum equal to 10^{16} cm^{-3}eV^{-1} and a standard deviation $\sigma_{DB}=0.15$ eV. The correlation energy E_u is equal to -0.3 eV. The other parameters are the same as in Sec. III A 2.

(a) Transition between the recombination-limited regime and the trapping- and release-limited regime. In Fig. 23 the dependence of $\cos(\Phi)/|I_{ac}|$ upon frequency at $T=400$ K for $G_{dc}=5\times10^{15}$ cm^{-3}s^{-1} and $G_{dc}=5\times10^{18}$ cm^{-3}s^{-1} is shown. On both curves the frequencies corresponding to $c_n n+c_p p$, ω_p, and ω_n, which are such that $c_n n+c_p p<\omega_p<\omega_n$, are indicated by a simple, a full, and an open arrow, respectively. It seems that the end of the plateau corresponds to none of these three values. However, the plot of $\tan(\Phi)$ versus the frequency presented in Fig. 24 shows that a deviation from the linear dependence occurs for angular frequencies above $c_n n+c_p p$. As a consequence, the following features can be outlined.

(i) In some cases the plot of $\cos(\Phi)/|I_{ac}|$ can lead to a wrong determination of the transition frequency. Indeed, $\cos(\Phi)/|I_{ac}|$ can appear independent of the frequency whereas the modulated photocurrent is neither in a pure recombination-limited regime nor in a pure trapping- and release-limited regime. The plot of $\tan(\Phi)$ versus frequency seems then to be more accurate.

(ii) In the presence of several species of traps, each of them having its own threshold frequency, the recombination-limited regime of the modulated photocurrent ends at the lowest of these threshold frequencies. It can be determined in the linear plot of $\tan(\Phi)$ versus

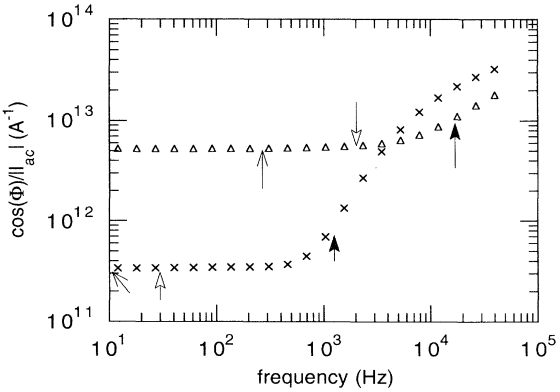

FIG. 23. Frequency dependence of $\cos(\Phi)/|I_{ac}|$ obtained at $T=400$ K for a low and high dc generation rate, (×) $G_{dc}=5\times10^{15}$ cm^{-3}s^{-1}, and (△) $G_{dc}=5\times10^{18}$ cm^{-3}s^{-1}. Both curves are normalized to an ac generation rate $G_{ac}=5\times10^{13}$ cm^{-3}s^{-1}. In both parts the simple, open, and full arrows indicate the transition frequencies corresponding to $2\pi f_{mono}=c_n n_{dc}+c_p p_{dc}$, $2\pi f_n=\omega_n$, and $2\pi f_p=\omega_p$, respectively. None of these values seems to corresponds to the end of the plateau.

the frequency. The higher the dc generation rate the more accurate this determination. From the measurement of this threshold frequency and the dc current value, it is possible to obtain an order of magnitude of the lowest capture coefficient. Furthermore, if there is one type of carrier giving a predominant contribution to both the dc current and the ac photocurrent, and if its mobility value is known, it is possible to deduce the lowest capture cross section of the states for this type of carrier from the measurements of the threshold frequency and of the dc current.

(b) DOS reconstruction in the trapping- and release-limited regime. Since there are clearly fewer states in the upper half of the gap than below midgap, and due to the higher mobility assumed for the electrons ($\mu_n = 10$ $cm^2 V^{-1} s^{-1}$ and $\mu_p = 1$ $cm^2 V^{-1} s^{-1}$), the modulated photocurrent is dominated by the electrons. Using the electron parameters for the D^+ centers, that is, using $v\sigma = c_n^+ = 2\times10^{-7}$ $cm^3 s^{-1}$, we have reconstructed the DOS by means of Eqs. (61) and (62). This is presented in Fig. 25 where each set of symbols corresponds to a different temperature. It is clear that a large part of the reconstructed DOS agrees well with the introduced one (full line for the DB states and dashed line for the band-tail states) except at energies close to midgap where the reconstructed DOS is quenched. Again, this quenching of the reconstructed DOS traduces the transition from the trapping- and release-limited regime to the recombination-limited regime. This behavior is identical to what is observed with monovalent states when the energy of the probed states falls below the Fermi level.[28] This shows, as it was done theoretically, that a distribution of DB states with a negative E_u and interacting with the conduction band behaves mainly as a distribution of monovalent states for which the capture coefficient would be c_n^+ and the Fermi level would be at $E_F - E_u/2$.

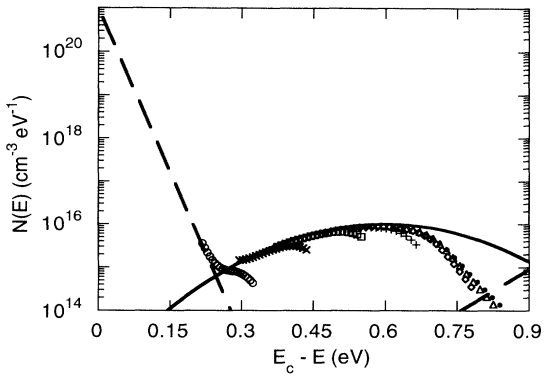

FIG. 25. The DOS reconstructed by means of Eqs. (61) and (62) (same symbols as in Fig. 13) is compared with the DOS introduced in the simulation (full line for the DB distribution and dashed line for the band tails). The correlation energy is $E_u = -0.3$ eV. The reconstructed DOS is calculated using $v\sigma = c_n^+$. The reconstruction is very good except for energies close to or below $E_F - E_u/2$. This is because under this energy limit DB states behave mainly as recombination centers for the considered carrier and not as traps.

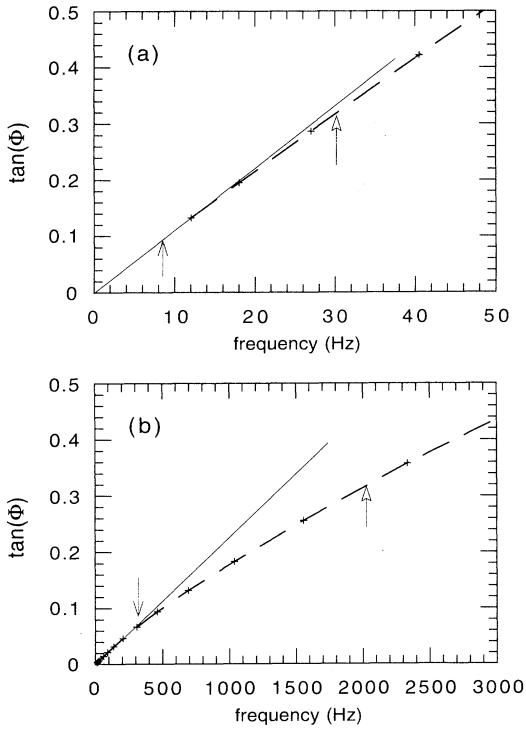

FIG. 24. Linear plot of tan(Φ) vs the modulation frequency at $T = 400$ K for the two cases considered in Fig. 23. In (a) $G_{dc} = 5\times10^{15}$ $cm^{-3} s^{-1}$ and in (b) $G_{dc} = 5\times10^{18}$ $cm^{-3} s^{-1}$. In both figures the transition frequencies corresponding to $2\pi f_{mono} = c_n n_{dc} + c_p p_{dc}$ and $2\pi f_n = \omega_n$ are reported with a simple and open arrow, respectively. For (a) the low dc generation rate, the end of the recombination-limited regime corresponds to a frequency between f_{mono} and f_n, whereas for (b) the high dc generation rate, the end of the recombination-limited regime corresponds to f_{mono}.

To study the interaction of a Gaussian distribution of DB states with the valence band we have reversed the DOS of the previous simulation, making a mirror symmetry around midgap. Hence we have $T_v = 200$ K, $T_c = 750$ K, $E_c - E_{DB} = 1.2$ eV, and $E_c - E_{F0} = 0.95$ eV. Considering this DOS it is clear that there are more states in the upper half of the gap than below midgap. The values of the mobilities were also exchanged ($\mu_p = 10$ $cm^2 V^{-1} s^{-1}$ and $\mu_n = 1$ $cm^2 V^{-1} s^{-1}$). Consequently, we expect to obtain a modulated photocurrent dominated by the holes. Using the hole parameters for the D^- centers, that is, using $v\sigma = c_p^- = 2\times10^{-7}$ $cm^3 s^{-1}$, we have reconstructed the DOS by means of Eqs. (61) and (62). The results are presented in Fig. 26 where each set of symbols corresponds to a different temperature. At first sight it seems that the reconstructed DOS (symbols) does not fit the introduced one (full line) at all. This is due to the fact that the reconstructed DOS is 0.3 eV ($= -E_u$) closer to the valence-band edge than the introduced one. Indeed, according to Eqs. (57) and (58) the major exchange of holes between the DB states and the valence band occurs at

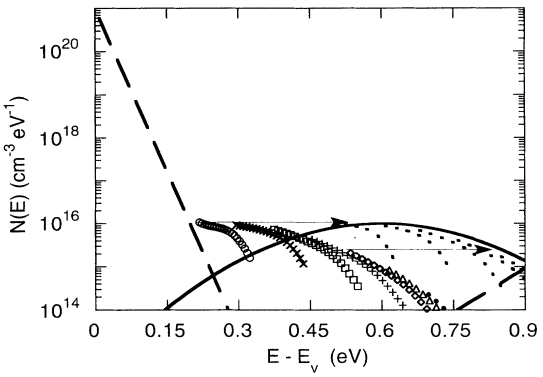

FIG. 26. The DOS reconstructed by means of Eqs. (61) and (62) (same symbols as in Fig. 13) is compared with the DOS introduced in the simulation (full line for the DB distribution and dashed line for the band tails). The correlation energy is $E_u=-0.3$ eV. The reconstructed DOS is calculated using $v\sigma=c_p^-$. The reconstruction is very good if the reconstructed DOS is shifted along the energy axis of a quantity equal to $-E_u$ (dotted lines).

$E^0_{\omega p}$. Therefore, a simple look at Eqs. (52) defining $E^0_{\omega p}$ and at Eq. (62) used to scale the energy axis shows that the reconstructed DOS must be translated along the energy axis to fit the introduced one, the amount of this translation being precisely equal to $-E_u$. As it could be deduced from our theoretical study, the distribution of DB states behaves as a distribution of monovalent centers with a capture coefficient equal to c_p^- located E_u closer to the valence-band edge than the actual position of the distribution of DB states.

In summary, if there is a predominant contribution of one type of carrier to the modulated photocurrent, a single distribution of negatively correlated DB centers behaves mainly as a distribution of monovalent centers with the appropriate capture cross sections. Conversely, if there is no clear cut between one type of carrier or the other, this result will be different. Indeed, a distribution of DB states peaked at $E_{\rm DB}$ can be roughly replaced by a distribution of monovalent states peaked at the same energy for describing the interactions with the electrons, while it has to be replaced by a distribution of monovalent states peaked at $E_{\rm DB}+E_u$ to describe the interactions with the holes. Therefore, as far as the modulated photocurrent is concerned, a single distribution of DB states with a negative correlation energy cannot be replaced by a single distribution of monovalent states if neither the electrons nor the holes are the predominant type of carriers because these monovalent centers cannot be peaked simultaneously at $E_{\rm DB}$ and $E_{\rm DB}+E_u$.

IV. CONCLUSIONS

Our development has brought some insight to the behavior and the determination of the DB states in amorphous and glassy semiconductors. Several issues have been successively addressed.

In a first step we have studied the occupation of the DB centers under steady-state illuminating conditions. For that purpose, the variations with respect to energy of the occupation functions f^+, f^-, and f^0 of the positively charged, negatively charged, and neutral dangling bonds have been calculated for both cases of the correlation energy ($E_u>0$ and $E_u<0$). We have shown that the concept of quasi-Fermi levels for trapped carriers introduced by Simmons and Taylor[22] for monovalent centers has to be reconsidered in the case of a distribution of DB states. In particular, if $E_u>0$, four energy levels have to be considered. These levels play the same role as the two quasi-Fermi levels for trapped carriers for monovalent centers, and simple constant values can be found for f^+, f^-, and f^0 within the intervals delimited by these new energy levels. The different recombination paths through the DB states have been clearly identified for both signs of the correlation energy and expressions of the lifetimes of the holes and of the electrons have been also deduced. It has been shown that, contrary to what can be found in the literature, these expressions do not consist in a simple extension to a distribution of DB states of the expressions proposed by Morgado[18] for a single discrete level of dangling bonds.

In a second step, we have focused on the influence of the DB centers on the modulated photocurrent and have addressed the determination of the expressions of the modulus and of the phase shift of the modulated photocurrent. A distinction has been made between a recombination-limited regime and a trapping- and release-limited regime of the modulated photocurrent depending on the frequency of the modulation.

In the high-frequency domain the modulated photocurrent is controlled by trapping and release processes. In that domain, many of the results obtained for a single distribution of monovalent states are valid for distributions of DB states. Thus we have underlined behaviors that are specific to the DB centers. Both theoretically and by means of our simulation, we have shown that a *single* distribution of DB states with a *positive* correlation energy can behave either as *two* distributions of monovalent states or as a *single* distribution of monovalent states depending on the relative positions of the dark Fermi level and of the DB states distribution. Another important result is that, if the modulated photocurrent is dominated by electrons, as it may be the case in *a*-Si:H, then it is possible to probe a distribution of DB states down to the correlation energy *below* the dark Fermi level. On the contrary, in the case of a *single* distribution of DB states with a *negative* correlation energy, this distribution behaves almost as a *single* distribution of monovalent centers.

In the low-frequency domains the modulated photocurrent is recombination limited. The upper limit of this domain is clearly identified by the end of the linear variations of $\tan(\Phi)$ versus the frequency of the modulation. As it was found for a DOS made of a single distribution of monovalent states, in the case of a modulated photocurrent due to a single type of carrier, this upper limit can lead to the determination of a capture coefficient if the DOS is made of a single distribution of DB with a *positive* correlation energy. In that case the capture

coefficients determined for the carrier considered correspond to that of the D^0. On the contrary, in the case of a distribution of DB with a *negative* correlation energy this upper limit can hardly be connected to any value of the capture coefficients. In any case, the determination of a capture coefficient from this upper limit is hardly possible in the case of a "real" DOS if many types of states are involved. However, an order of magnitude of the *lowest* capture coefficient of the gap states can be obtained.

Moreover, even if several types of states are involved, we believe that, considering the theoretical outlines developed in this paper, a good understanding of the DOS in amorphous and glassy semiconductors should be possible by combining experimental results with those derived from the simulation.

ACKNOWLEDGMENTS

Laboratoire de Génie Electrique de Paris is "Unité Associée au Centre National de la Recherche Scientifique No. D0127." We gratefully acknowledge the help of Professor G. Fournet in many stimulating discussions.

APPENDIX A: EXPRESSION OF THE COEFFICIENTS OF THE OCCUPATION FUNCTIONS OF THE DANGLING BONDS

The whole calculation of the coefficients of n_r, n_i, p_r, and p_i for f_{ac}^+, f_{ac}^0, and f_{ac}^- is quite long and tedious, though the calculation in itself does not present any mathematical difficulties. Basically it consists in the resolution of a system of three equations with three unknown quantities. So we shall not go into too much detail.

We define the energy-dependent quantities A, B, and Δ by

$$\begin{aligned} A&=(P^0P^-+N^+P^-+N^0N^+-\omega^2)\ , \\ B&=\omega(P^0+P^-+N^++N^0)\ , \\ \Delta&=(P^0P^-+N^+P^-+N^0N^+-\omega^2)^2 \\ &\quad+\omega^2(P^0+P^-+N^++N^0)^2\ . \end{aligned} \tag{A1}$$

The coefficients of n_r, n_i, p_r, and p_i for $f_{ac}^+(E)$ are

$$\alpha_n^+(E)=-\frac{\{P^0Ac_n^0f_{dc}^0+[(P^-+N^0)A+\omega B]c_n^+f_{dc}^+\}}{\Delta}\ , \tag{A2}$$

$$\beta_n^+(E)=\frac{\{-P^0Bc_n^0f_{dc}^0+[\omega A-(P^-+N^0)B]c_n^+f_{dc}^+\}}{\Delta}\ , \tag{A3}$$

$$\alpha_p^+(E)=\frac{\{P^0Ac_p^-f_{dc}^-+[(P^-+N^0)A+\omega B]c_p^0f_{dc}^0\}}{\Delta}\ , \tag{A4}$$

$$\beta_p^+(E)=\frac{\{P^0Bc_p^-f_{dc}^--[\omega A-(P^-+N^0)B]c_p^0f_{dc}^0\}}{\Delta}\ . \tag{A5}$$

The coefficients of n_r, n_i, p_r, and p_i for $f_{ac}^0(E)$ are

$$\alpha_n^0(E)=\frac{[-(N^+A+\omega B)c_n^0f_{dc}^0+(P^-A+\omega B)c_n^+f_{dc}^+]}{\Delta}\ , \tag{A6}$$

$$\beta_n^0(E)=\frac{[-(N^+B-\omega A)c_n^0f_{dc}^0+(P^-B-\omega A)c_n^+f_{dc}^+]}{\Delta}\ , \tag{A7}$$

$$\alpha_p^0(E)=\frac{[(N^+A+\omega B)c_p^-f_{dc}^--(P^-A+\omega B)c_p^0f_{dc}^0]}{\Delta}\ , \tag{A8}$$

$$\beta_p^0(E)=\frac{[(N^+B-\omega A)c_p^-f_{dc}^--(P^-B-\omega A)c_p^0f_{dc}^0]}{\Delta}\ . \tag{A9}$$

On the right-hand side of Eqs. (A1)–(A9), we have not indicated the energy dependence of the terms for the sake of clarity. The coefficients of n_r, n_i, p_r, and p_i for f_{ac}^- can be deduced from the coefficients of f_{ac}^+ by application of the transformation $\mathcal{T}$ to the expression of f_{ac}^+. Note that the expressions of A, B, and Δ are unchanged by $\mathcal{T}$.

APPENDIX B: DETERMINATION OF THE LIMITS OF THE INTERVALS OF VARIATIONS OF THE OCCUPATION FUNCTIONS FOR $E_u>0$

In the case $E_u>0$ the fundamental intervals for the variation of the occupation functions are delimited by the energy levels E_{tn}^-, E_{tn}^0, E_{tp}^0, and E_{tp}^+. The first interval where $E_{tn}^0<E<E_c$ is defined by

$$\begin{aligned} &e_n^-(E)>\bar{n}_{dc}^0+\bar{p}_{dc}^-,\quad e_p^+(E)<\bar{p}_{dc}^0+\bar{n}_{dc}^+\ , \\ &e_n^0(E)>\bar{n}_{dc}^++\bar{p}_{dc}^0,\quad e_p^0(E)<\bar{p}_{dc}^-+\bar{n}_{dc}^0\ , \end{aligned} \tag{B1}$$

and the second interval, where $E<E_{tn}^0$, $E>E_{tp}^+$, $E>E_{tn}^-$, and $E>E_{tp}^0$ is defined by

$$\begin{aligned} &e_n^-(E)>\bar{n}_{dc}^0+\bar{p}_{dc}^-,\quad e_p^+(E)<\bar{p}_{dc}^0+\bar{n}_{dc}^+\ , \\ &e_n^0(E)<\bar{n}_{dc}^++\bar{p}_{dc}^0,\quad e_p^0(E)<\bar{p}_{dc}^-+\bar{n}_{dc}^0\ . \end{aligned} \tag{B2}$$

As far as the third interval is concerned, in the case (1,2,3,4,5) where $E_{tp}^0<E_{tp}^+<E<E_{tn}^-<E_{tn}^0$, we can write

$$\begin{aligned} &e_n^-(E)<\bar{n}_{dc}^0+\bar{p}_{dc}^-,\quad e_p^+(E)<\bar{p}_{dc}^0+\bar{n}_{dc}^+\ , \\ &e_n^0(E)<\bar{n}_{dc}^++\bar{p}_{dc}^0,\quad e_p^0(E)<\bar{p}_{dc}^-+\bar{n}_{dc}^0\ , \end{aligned} \tag{B3}$$

and in the case (1,2,3′,4,5), where $E_{tp}^0<E_{tn}^-<E<E_{tp}^+<E_{tn}^0$,

$$\begin{aligned} &e_n^-(E)>\bar{n}_{dc}^0+\bar{p}_{dc}^-,\quad e_p^+(E)>\bar{p}_{dc}^0+\bar{n}_{dc}^+\ , \\ &e_n^0(E)<\bar{n}_{dc}^++\bar{p}_{dc}^0,\quad e_p^0(E)<\bar{p}_{dc}^-+\bar{n}_{dc}^0\ . \end{aligned} \tag{B4}$$

Finally, for the fourth interval where $E>E_{tp}^0$, $E<E_{tn}^-$, $E<E_{tp}^+$, and $E<E_{tn}^0$, we have

$$e_n^-(E)<\bar{n}_{dc}^0+\bar{p}_{dc}^-,\quad e_p^+(E)>\bar{p}_{dc}^0+\bar{n}_{dc}^+,$$
$$e_n^0(E)<\bar{n}_{dc}^++\bar{p}_{dc}^0,\quad e_p^0(E)<\bar{p}_{dc}^-+\bar{n}_{dc}^0, \tag{B5}$$

and for the fifth interval, where $E_v<E<E_{tp}^0$,

$$e_n^-(E)<\bar{n}_{dc}^0+\bar{p}_{dc}^-,\quad e_p^+(E)>\bar{p}_{dc}^0+\bar{n}_{dc}^+,$$
$$e_n^0(E)<\bar{n}_{dc}^++\bar{p}_{dc}^0,\quad e_p^0(E)>\bar{p}_{dc}^-+\bar{n}_{dc}^0. \tag{B6}$$

Note that this last interval may be nonexistent. Indeed, if p_{dc} is high, then E_{Fp} is close to the valence band. Since E_{tp}^+ is close to E_{Fp}, a large E_u results in E_{tp}^0 lower than E_v.

APPENDIX C: EXPRESSIONS OF THE COEFFICIENTS OF THE SYSTEM (33) OF FOUR EQUATIONS

The expressions of the coefficients of the system (33) are

$$A_n^{DB}=-\int_{E_v}^{E_c}\{\alpha_n^-(E)e_n^-(E)-\alpha_n^+(E)\bar{n}_{dc}^+ -\alpha_n^0(E)[\bar{n}_{dc}^0-e_n^0(E)]\}N^{DB}(E)dE +\int_{E_v}^{E_c}[c_n^+f_{dc}^+(E)+c_n^0f_{dc}^0(E)]N^{DB}(E)dE, \tag{C1}$$

$$B_n^{DB}=\int_{E_v}^{E_c}\{\beta_n^-(E)e_n^-(E)-\beta_n^+(E)\bar{n}_{dc}^+ -\beta_n^0(E)[\bar{n}_{dc}^0-e_n^0(E)]\}N^{DB}(E)dE, \tag{C2}$$

$$A_p^{*DB}=-\int_{E_v}^{E_c}\{\alpha_p^-(E)e_n^-(E)-\alpha_p^+(E)\bar{n}_{dc}^+ -\alpha_p^0(E)[\bar{n}_{dc}^0-e_n^0(E)]\}N^{DB}(E)dE, \tag{C3}$$

$$B_p^{*DB}=-\int_{E_v}^{E_c}\{\beta_p^-(E)e_n^-(E)-\beta_p^+(E)\bar{n}_{dc}^+ -\beta_p^0(E)[\bar{n}_{dc}^0-e_n^0(E)]\}N^{DB}(E)dE. \tag{C4}$$

The expressions of A_n^{*DB}, B_n^{*DB}, A_p^{DB}, and B_p^{DB} can be deduced by means of the transformation $\mathcal{T}$ applied to the expressions of A_p^{*DB}, B_p^{*DB}, A_n^{DB}, and B_n^{DB}, respectively. If several species of gap states are taken into account, the coefficients of n_r, n_i, p_r, and p_i in the system (33) have to reflect their respective contributions. For instance, if one considers that the DOS is made of M species of DB states and N species of monovalent states, the coefficient of n_r in the first line of system (33) becomes

$$A_n=\sum_{i=1}^{M}[A_n^{DB}]_i+\sum_{j=1}^{N}[A_n^{mono}]_j. \tag{C5}$$

$[A_n^{DB}]_i$ is the coefficient relative to the ith species of DB states which can be calculated from Eq. (C1) by using the characteristics (capture cross sections, correlation energy) of this type of defect. $[A_n^{mono}]_j$ is the coefficient relative to the jth species of monovalent states and can be calculated from the expressions given in a previous paper.[28] Note that, compared with this previous paper, our notations have been slightly modified in order to make them compatible with the use of the $\mathcal{T}$ transform. The other coefficients involved in the system (33) can be obtained in the same way by equations analogous to Eq. (C5).

[1]M. H. Cohen, H. Fritzsche, and S. R. Ovshinsky, Phys. Rev. Lett. **22**, 1065 (1969).
[2]N. F. Mott, Adv. Phys. **16**, 49 (1967).
[3]R. A. Street and N. F. Mott, Phys. Rev. Lett. **35**, 1293 (1975).
[4]G. J. Adriaenssens, Philos. Mag. B **62**, 79 (1990).
[5]D. Adler, Phys. Rev. Lett. **41**, 1755 (1978).
[6]J. K. Lee and E. A. Schiff, Phys. Rev. Lett. **68**, 2972 (1992).
[7]M. Stutzmann, Philos. Mag. B **60**, 531 (1989).
[8]K. Winer, Phys. Rev. B **41**, 12 150 (1990).
[9]D. Redfield and H. Bube, J. Non-Cryst. Solids **137&138**, 215 (1991).
[10]N. Hata and S. Wagner, J. Appl. Phys. **72**, 2857 (1992).
[11]F. Vaillant and D. Jousse, Phys. Rev. B **34**, 4088 (1986).
[12]H. Okamoto, H. Kida, and Y. Hamakawa, Philos. Mag. B **49**, 231 (1984).
[13]J. Hubin, A. V. Shah, and E. Sauvain, Philos. Mag. B **66**, 115 (1992).
[14]R. A. Street, J. Kakalios, C. C. Tsaï, and T. M. Hayes, Phys. Rev. B **35**, 1316 (1987).
[15]M. Meaudre, P. Jensen, and R. Meaudre, Philos. Mag. B **63**, 815 (1991).
[16]Z. E. Smith, S. Aljishi, D. Slobodin, V. Chu, S. Wagner, P. M. Lenahan, R. R. Arya, and M. S. Bennett, Phys. Rev. Lett. **57**, 2450 (1986).
[17]K. Zellama, H. Labida, P. Germain, H. J. von Bardeleben, L. Chahed, M. L. Theye, P. Roca i Cabarrocas, C. Godet, and J. P. Stoquert, Phys. Rev. B **45**, 13 314 (1992).
[18]E. Morgado, Philos. Mag. B **63**, 529 (1991).
[19]D. Adler and E. J. Yoffa, Phys. Rev. Lett. **36**, 1197 (1976).
[20]H. Okamoto and Y. Hamakawa, Solid State Commun. **24**, 23 (1977).
[21]S. Lee, M. Gunes, C. R. Wronsky, N. Maley, and M. Bennet, Appl. Phys. Lett. **59**, 1578 (1991).
[22]J. G. Simmons and G. W. Taylor, Phys. Rev. B **4**, 502 (1971).
[23]H. Oheda, J. Appl. Phys. **52**, 6693 (1981).
[24]G. Schumm and G. H. Bauer, Phys. Rev. B **39**, 5311 (1989).
[25]J. P. Kleider, C. Longeaud, and O. Glodt, J. Non-Cryst. Solids **137&138**, 447 (1992).
[26]R. Brüggemann, C. Main, J. Berkin, and S. Reynolds, Philos. Mag. B **62**, 29 (1990).
[27]C. Main, D. P. Webb, R. Brüggemann, and S. Reynolds, J. Non-Cryst. Solids **137&138**, 951 (1992).
[28]C. Longeaud and J. P. Kleider, Phys. Rev. B **45**, 11 672 (1992).
[29]L. Schweitzer, M. Grünewald, and H. Dersch, Solid State Commun. **39**, 355 (1981).
[30]G. W. Taylor and J. G. Simmons, J. Non-Cryst. Solids **8–10**, 940 (1972).
[31]W. Shockley and W. T. Read, Phys. Rev. **87**, 835 (1952).
[32]F. Vaillant, D. Jousse, and J. C. Bruyère, Philos. Mag. B **57**, 649 (1988).
[33]V. Halpern, Philos. Mag. B **54**, 473 (1986).
[34]J. M. Essick and J. D. Cohen, Phys. Rev. Lett. **64**, 3062 (1990).

[35]Moreover, if the reader wants to study a particular point we can send him or her a copy of the software we used to perform our simulation.
[36]V. Premachandran, K. L. Narasimhan, and D. R. Bapat, Phys. Rev. B **29**, 7073 (1984).
[37]J. Tardy and R. Meaudre, Solid State Commun. **39**, 1031 (1981).
[38]R. A. Street and D. K. Biegelsen, J. Non-Cryst. Solids **35&36**, 651 (1980).